Journal of Computational Physics 258 (2014) 915–930

Contents lists available at ScienceDirect

Journal of Computational Physics

www.elsevier.com/locate/jcp

Analysis and application of the nodal discontinuous Galerkin method for wave propagation in metamaterials

Jichun Li [a,*,1], Jan S. Hesthaven [b]

[a] Department of Mathematical Sciences, University of Nevada Las Vegas, Las Vegas, Nevada 89154-4020, USA
[b] EPFL-SB-MATHICSE-MCSS, Ecole Polytechnique Fédérale de Lausanne (EPFL), CH-1015 Lausanne, Switzerland

ARTICLE INFO

Article history:
Received 30 December 2012
Received in revised form 5 November 2013
Accepted 15 November 2013
Available online 20 November 2013

Keywords:
Maxwell's equations
Metamaterial
Discontinuous Galerkin method
Perfectly matched layers

ABSTRACT

In this paper, we develop a nodal discontinuous Galerkin method for solving the time-dependent Maxwell's equations when metamaterials are involved. Both semi- and fully-discrete schemes are constructed. Numerical stability and error estimate are proved for both schemes. Numerical results are presented to demonstrate that the method is not only efficient but also very effective in solving metamaterial Maxwell's equations.

1. Introduction

Since early 2000s, the discontinuous Galerkin (DG) method [2] has become one of the most popular methods in solving various differential equations (e.g., [1,7,18,21,23]) due to its flexibility in mesh construction and its convenience in parallel implementation. In the mean time, there have been considerable interests in developing DG methods for Maxwell's equations in free space [3–6,8,9,11,20]. Very recently, there are some DG work [19,13,25] carried out for Maxwell's equations in dispersive media, whose permittivity depends on the wave frequency. However, the study of DG method for Maxwell's equations in metamaterials is quite limited, except our recent works [14,17].

The metamaterials are artificially structured electromagnetic composite materials with some exotic properties such as negative refractive index and amplification of evanescent waves. Intensive study of metamaterials started around 2000, immediately after the successful construction of such a metamaterial by Smith et al. [22]. Many potentially revolutionary applications (such as construction of perfect lens, sub-wavelength imaging and cloaking devices) have attracted researchers from many areas to work in metamaterials. Numerical simulation plays a very important role in the study of metamaterials. However, such simulations are almost exclusively based on either the classic finite-difference time-domain (FDTD) method or commercial packages such as COMSOL, a multiphysics finite element package. Due to the constraint of FDTD method (e.g., difficult in handling the complex geometries) and the black-box characteristics of commercial packages, there is an urgent call for developing more efficient and reliable software for metamaterial simulations. In recent years, we made some initial effort [14–16] in developing and analyzing some finite element methods (FEM) for solving the time-domain Maxwell's equations in metamaterials.

This paper continues our initial effort [14,17] on developing time-domain DG methods for solving the Maxwell's equations in metamaterials. In [14], we extended the nodal DG method of Hesthaven and Warburton [9,10] to metamaterial

* Corresponding author. Tel.: +1 702 895 0355.
E-mail addresses: jichun@unlv.nevada.edu (J. Li), jan.hesthaven@epfl.ch (J.S. Hesthaven).
[1] Supported by NSF grant DMS-0810896.

0021-9991/$ – see front matter
http://dx.doi.org/10.1016/j.jcp.2013.11.018

Maxwell's equations and performed some numerical tests with upwind flux and the classic fourth-order explicit Runge–Kutta (RK) method. We did not perform any stability and error analysis for the DG method in [14]. Later in [17], we proposed a leap-frog DG scheme with upwind flux for solving the same model problem as [14]. In [17], we also proved the numerical stability and the error estimate $O(\tau^2+h^k)$ in the $L^\infty(0,T;(L^2(\Omega))^3)$ norm, where τ is the time step size, h is the mesh size, and k is the order of the basis function. Numerical tests in [17] showed the optimal convergence rate $O(h^{k+1})$, but the rigorous proof of this fact is still open. In this paper, we propose another leap-frog DG method based on the central flux. Compared to [17], this new scheme enjoys simpler and more efficient implementation, and a more succinct proof for the stability and error estimate. Furthermore, practical numerical simulation of backward wave propagation phenomenon is also demonstrated using this newly developed nodal DG method.

The rest of the paper is organized as follows. In Section 2, we first present the governing equations for metamaterials, and then develop both semi- and full-discrete nodal DG methods for the metamaterial Maxwell's equations. Stability and error analysis are provided. In Section 3, we extend the algorithm and analysis to a perfectly matched layer (PML) model, which is used for the simulation of backward wave propagation in metamaterials. In Section 4, numerical results are presented to support our theoretical analysis and demonstrate the efficiency and effectiveness of the nodal DG method for modeling wave propagation in metamaterials. Section 5 concludes the paper.

2. The DG method for metamaterials

2.1. The governing equations

The governing equations for modeling wave propagation in metamaterials are [14]:

$$\epsilon_0\frac{\partial \boldsymbol{E}}{\partial t}=\nabla\times\boldsymbol{H}-\boldsymbol{J},\quad \text{in } \Omega\times(0,T), \tag{1}$$

$$\mu_0\frac{\partial \boldsymbol{H}}{\partial t}=-\nabla\times\boldsymbol{E}-\boldsymbol{K},\quad \text{in } \Omega\times(0,T), \tag{2}$$

$$\frac{\partial \boldsymbol{J}}{\partial t}+\Gamma_e\boldsymbol{J}=\epsilon_0\omega_{pe}^2\boldsymbol{E},\quad \text{in } \Omega\times(0,T), \tag{3}$$

$$\frac{\partial \boldsymbol{K}}{\partial t}+\Gamma_m\boldsymbol{K}=\mu_0\omega_{pm}^2\boldsymbol{H},\quad \text{in } \Omega\times(0,T), \tag{4}$$

where ϵ_0 and μ_0 denote the vacuum permittivity and permeability, ω_{pe} and ω_{pm} are the electric and magnetic plasma frequencies, respectively, Γ_e and Γ_m are the electric and magnetic damping frequencies, respectively, $\boldsymbol{E}(\boldsymbol{x},t)$ and $\boldsymbol{H}(\boldsymbol{x},t)$ are the electric and magnetic fields, respectively, and $\boldsymbol{J}(\boldsymbol{x},t)$ and $\boldsymbol{K}(\boldsymbol{x},t)$ are the induced electric and magnetic currents, respectively. Here Ω is assumed to be a bounded Lipschitz polyhedral domain in $\mathcal{R}^d$ ($d=2$ or 3) with connected boundary $\partial\Omega$. To make the problem well-posed, we further assume that the system (1)–(4) is subject to the perfectly conducting boundary condition:

$$\hat{\boldsymbol{n}}\times\boldsymbol{E}=0\quad \text{on } \partial\Omega, \tag{5}$$

where $\hat{\boldsymbol{n}}$ is the unit outward normal to $\partial\Omega$, and the initial conditions:

$$\boldsymbol{E}(\mathbf{x},0)=\boldsymbol{E}_0(\mathbf{x}),\qquad \boldsymbol{H}(\mathbf{x},0)=\boldsymbol{H}_0(\mathbf{x}), \tag{6}$$

$$\boldsymbol{J}(\mathbf{x},0)=\boldsymbol{J}_0(\mathbf{x}),\qquad \boldsymbol{K}(\mathbf{x},0)=\boldsymbol{K}_0(\mathbf{x}), \tag{7}$$

where $\boldsymbol{E}_0$, $\boldsymbol{H}_0$, $\boldsymbol{J}_0$ and $\boldsymbol{K}_0$ are some given functions.

2.2. The semi-discrete DG method

To discretize the system (1)–(4), we consider a shape-regular mesh T_h that partitions the domain Ω into N_T disjoint triangular or tetrahedral elements T_i such that $\overline{\Omega}=\bigcup_{i=1}^{N_T}T_i$. Furthermore, we denote $a_{ik}=T_i\cap T_k$ for an interior face between two adjacent elements T_i and T_k, and $\boldsymbol{n}_{ik}$ for the unit normal vector pointed from T_i to T_k. For any given element T_i, we denote ν_i for the set of all neighboring elements of T_i.

In DG methods, we consider the discretization space given by discontinuous piecewise polynomials of degree k on each element, i.e.,

$$\boldsymbol{V}_h=\left\{\boldsymbol{v}_h\in\left(L^2(\Omega)\right)^d:\ \boldsymbol{v}_h|_{T_i}\in(P_k)^d,\ \forall T_i\in T_h\right\},\quad d=2 \text{ or } 3.$$

Multiplying Eqs. (1)–(4) by test functions $\boldsymbol{u},\boldsymbol{v},\boldsymbol{\phi},\boldsymbol{\psi}$, respectively, and integrating by parts over any element $T_i\in T_h$, we have

$$\epsilon_0 \int_{T_i} \frac{\partial \boldsymbol{E}}{\partial t} \cdot \boldsymbol{u} - \int_{T_i} \boldsymbol{H} \cdot \nabla \times \boldsymbol{u} - \int_{\partial T_i} \boldsymbol{n}_i \times \boldsymbol{H} \cdot \boldsymbol{u} + \int_{T_i} \boldsymbol{J} \cdot \boldsymbol{u} = 0, \tag{8}$$

$$\mu_0 \int_{T_i} \frac{\partial \boldsymbol{H}}{\partial t} \cdot \boldsymbol{v} + \int_{T_i} \boldsymbol{E} \cdot \nabla \times \boldsymbol{v} + \int_{\partial T_i} \boldsymbol{n}_i \times \boldsymbol{E} \cdot \boldsymbol{v} + \int_{T_i} \boldsymbol{K} \cdot \boldsymbol{v} = 0, \tag{9}$$

$$\frac{1}{\epsilon_0 \omega_{pe}^2} \int_{T_i} \frac{\partial \boldsymbol{J}}{\partial t} \cdot \boldsymbol{\phi} + \frac{\Gamma_e}{\epsilon_0 \omega_{pe}^2} \int_{T_i} \boldsymbol{J} \cdot \boldsymbol{\phi} - \int_{T_i} \boldsymbol{E} \cdot \boldsymbol{\phi} = 0, \tag{10}$$

$$\frac{1}{\mu_0 \omega_{pm}^2} \int_{T_i} \frac{\partial \boldsymbol{K}}{\partial t} \cdot \boldsymbol{\psi} + \frac{\Gamma_m}{\mu_0 \omega_{pm}^2} \int_{T_i} \boldsymbol{K} \cdot \boldsymbol{\psi} - \int_{T_i} \boldsymbol{H} \cdot \boldsymbol{\psi} = 0. \tag{11}$$

Let us look at the semi-discrete solution $\boldsymbol{E}_h, \boldsymbol{H}_h, \boldsymbol{J}_h, \boldsymbol{K}_h \in C^1(0, T; \boldsymbol{V}_h)$ as a solution of the following weak formulation: For any $\boldsymbol{u}_h, \boldsymbol{v}_h, \boldsymbol{\phi}_h, \boldsymbol{\psi}_h \in \boldsymbol{V}_h$, and any element $T_i \in T_h$,

$$\epsilon_0 \int_{T_i} \frac{\partial \boldsymbol{E}_h}{\partial t} \cdot \boldsymbol{u}_h - \int_{T_i} \boldsymbol{H}_h \cdot \nabla \times \boldsymbol{u}_h - \sum_{K \in \nu_i} \int_{a_{ik}} \boldsymbol{u}_h \cdot \boldsymbol{n}_{ik} \times \{\{\boldsymbol{H}_h\}\}_{ik} + \int_{T_i} \boldsymbol{J}_h \cdot \boldsymbol{u}_h = 0, \tag{12}$$

$$\mu_0 \int_{T_i} \frac{\partial \boldsymbol{H}_h}{\partial t} \cdot \boldsymbol{v}_h + \int_{T_i} \boldsymbol{E}_h \cdot \nabla \times \boldsymbol{v}_h + \sum_{K \in \nu_i} \int_{a_{ik}} \boldsymbol{v}_h \cdot \boldsymbol{n}_{ik} \times \{\{\boldsymbol{E}_h\}\}_{ik} + \int_{T_i} \boldsymbol{K}_h \cdot \boldsymbol{v}_h = 0, \tag{13}$$

$$\frac{1}{\epsilon_0 \omega_{pe}^2} \int_{T_i} \frac{\partial \boldsymbol{J}_h}{\partial t} \cdot \boldsymbol{\phi}_h + \frac{\Gamma_e}{\epsilon_0 \omega_{pe}^2} \int_{T_i} \boldsymbol{J}_h \cdot \boldsymbol{\phi}_h - \int_{T_i} \boldsymbol{E}_h \cdot \boldsymbol{\phi}_h = 0, \tag{14}$$

$$\frac{1}{\mu_0 \omega_{pm}^2} \int_{T_i} \frac{\partial \boldsymbol{K}_h}{\partial t} \cdot \boldsymbol{\psi}_h + \frac{\Gamma_m}{\mu_0 \omega_{pm}^2} \int_{T_i} \boldsymbol{K}_h \cdot \boldsymbol{\psi}_h - \int_{T_i} \boldsymbol{H}_h \cdot \boldsymbol{\psi}_h = 0, \tag{15}$$

hold true and are subject to the initial conditions:

$$\boldsymbol{E}_h(0) = \Pi_2 \boldsymbol{E}_0(\boldsymbol{x}), \qquad \boldsymbol{H}_h(0) = \Pi_2 \boldsymbol{H}_0(\boldsymbol{x}), \qquad \boldsymbol{J}_h(0) = \Pi_2 \boldsymbol{J}_0(\boldsymbol{x}), \qquad \boldsymbol{K}_h(0) = \Pi_2 \boldsymbol{K}_0(\boldsymbol{x}), \tag{16}$$

where Π_2 denotes the standard L^2-projection onto $\boldsymbol{V}_h$. Here and below, for any function $\boldsymbol{v}_h$, we denote the average and jump through any internal face a_{ik} as

$$\{\{\boldsymbol{v}_h\}\}_{ik} = \frac{1}{2}(\boldsymbol{v}_i + \boldsymbol{v}_k), \qquad [\![\boldsymbol{v}_h]\!]_{ik} = (\boldsymbol{v}_k - \boldsymbol{v}_i).$$

Note that the perfectly conducting boundary condition (5) is treated as $\boldsymbol{E}_k|_{a_{ik}} = -\boldsymbol{E}_i|_{a_{ik}}$ and $\boldsymbol{H}_k|_{a_{ik}} = \boldsymbol{H}_i|_{a_{ik}}$, which lead to

$$\{\{\boldsymbol{E}\}\}_{ik} = 0, \quad \text{and} \quad \{\{\boldsymbol{H}\}\}_{ik} = \boldsymbol{H}_i|_{a_{ik}} \quad \text{for any } a_{ik} \in \partial\Omega.$$

Here and below we denote $\boldsymbol{E}_i = \boldsymbol{E}_h|_{T_i}$, $\boldsymbol{H}_i = \boldsymbol{H}_h|_{T_i}$, $\boldsymbol{J}_i = \boldsymbol{J}_h|_{T_i}$ and $\boldsymbol{K}_i = \boldsymbol{K}_h|_{T_i}$.

Denote the semi-discrete energy $\mathcal{E}_h$:

$$\mathcal{E}_h(t) = \frac{1}{2}\left(\epsilon_0 \left\|\boldsymbol{E}_h(t)\right\|_{0,\Omega}^2 + \mu_0 \left\|\boldsymbol{H}_h(t)\right\|_{0,\Omega}^2 + \frac{1}{\epsilon_0 \omega_{pe}^2} \left\|\boldsymbol{J}_h(t)\right\|_{0,\Omega}^2 + \frac{1}{\mu_0 \omega_{pm}^2} \left\|\boldsymbol{K}_h(t)\right\|_{0,\Omega}^2\right), \tag{17}$$

and a bilinear form $\mathcal{B}_i$:

$$\mathcal{B}_i(\boldsymbol{E}, \boldsymbol{H}) = -\int_{T_i} \boldsymbol{H}_i \cdot \nabla \times \boldsymbol{E}_i - \sum_{K \in \nu_i} \int_{a_{ik}} \boldsymbol{E}_h \cdot \boldsymbol{n}_{ik} \times \{\{\boldsymbol{H}_h\}\}_{ik} + \int_{T_i} \boldsymbol{E}_i \cdot \nabla \times \boldsymbol{H}_i + \sum_{K \in \nu_i} \int_{a_{ik}} \boldsymbol{H}_h \cdot \boldsymbol{n}_{ik} \times \{\{\boldsymbol{E}_h\}\}_{ik}. \tag{18}$$

Theorem 2.1. *The energy $\mathcal{E}_h$ is decreasing in time, i.e., $\mathcal{E}_h(t) \leqslant \mathcal{E}_h(0)$ for any $t \in [0, T]$.*

Proof. Choosing $\boldsymbol{u}_h = \boldsymbol{E}_h, \boldsymbol{v}_h = \boldsymbol{H}_h, \boldsymbol{\phi}_h = \boldsymbol{J}_h, \boldsymbol{\psi}_h = \boldsymbol{K}_h$ in (12)–(15), respectively, and adding the results over all elements T_i of T_h, we obtain

$$\frac{d}{dt}\mathcal{E}_h(t) + \frac{\Gamma_e}{\epsilon_0 \omega_{pe}^2} \left\|\boldsymbol{J}_h(t)\right\|_{0,\Omega}^2 + \frac{\Gamma_m}{\mu_0 \omega_{pm}^2} \left\|\boldsymbol{K}_h(t)\right\|_{0,\Omega}^2 + \sum_i \mathcal{B}_i(\boldsymbol{E}, \boldsymbol{H}) = 0. \tag{19}$$

Using the definition of $\mathcal{B}_i$, integration by parts, and the identity $(\mathbf{a} \times \mathbf{b}) \cdot \mathbf{c} = \mathbf{a} \cdot (\mathbf{b} \times \mathbf{c})$, we have

$$\begin{aligned}\mathcal{B}_i(\boldsymbol{E},\boldsymbol{H}) &= \sum_{K\in\nu_i}\int_{a_{ik}} \boldsymbol{E}_i\cdot\boldsymbol{n}_{ik}\times\boldsymbol{H}_i + \sum_{K\in\nu_i}\int_{a_{ik}} \boldsymbol{E}_i\cdot\{\{\boldsymbol{H}_h\}\}_{ik}\times\boldsymbol{n}_{ik} - \sum_{K\in\nu_i}\int_{a_{ik}} \boldsymbol{H}_i\cdot\{\{\boldsymbol{E}_h\}\}_{ik}\times\boldsymbol{n}_{ik}\\ &= \sum_{K\in\nu_i}\int_{a_{ik}}\left[-\boldsymbol{E}_i\times\boldsymbol{H}_i+\boldsymbol{E}_i\times\frac{\boldsymbol{H}_i+\boldsymbol{H}_k}{2}-\boldsymbol{H}_i\times\frac{\boldsymbol{E}_i+\boldsymbol{E}_k}{2}\right]\cdot\boldsymbol{n}_{ik}\\ &= \frac{1}{2}\sum_{K\in\nu_i}\int_{a_{ik}}(\boldsymbol{E}_i\times\boldsymbol{H}_k+\boldsymbol{E}_k\times\boldsymbol{H}_i)\cdot\boldsymbol{n}_{ik}. \end{aligned}\tag{20}$$

Summing up (20) over all elements of T_h, we obtain $\sum_i \mathcal{B}_i(\boldsymbol{E},\boldsymbol{H})=0$. The proof is completed by substituting this fact into (19). □

For the semi-discrete scheme (12)–(15), we have the following convergence result [16, Theorem 4.6].

Theorem 2.2. *If $\boldsymbol{E},\boldsymbol{H},\boldsymbol{J},\boldsymbol{K}\in C^0([0,T];(H^{s+1}(\Omega))^d)$ for $s\geqslant 0$, then there exists a constant $C>0$, independent of h, such that*

$$\begin{aligned}&\max_{t\in[0,T]}\left(\|\boldsymbol{E}-\boldsymbol{E}_h\|_{0,\Omega}+\|\boldsymbol{H}-\boldsymbol{H}_h\|_{0,\Omega}+\|\boldsymbol{J}-\boldsymbol{J}_h\|_{0,\Omega}+\|\boldsymbol{K}-\boldsymbol{K}_h\|_{0,\Omega}\right)\\ &\quad\leqslant Ch^{\min(s,k)}\left\|(\boldsymbol{E},\boldsymbol{H},\boldsymbol{J},\boldsymbol{K})\right\|_{C^0([0,T];(H^{s+1}(\Omega))^d)}.\end{aligned}\tag{21}$$

2.3. The fully-discrete DG method

To define a fully discrete scheme, we divide the time interval $(0,T)$ into N uniform subintervals by points $0=t_0<t_1<\cdots<t_N=T$, where $t_k=k\tau$, and $\tau=T/N$.

Following the idea of our previous work on leap-frog scheme [15,17], we can construct a leap-frog DG scheme as follows: Given initial approximations of $\boldsymbol{E}_h^0$, $\boldsymbol{H}_h^{\frac12}$, $\boldsymbol{J}_h^{\frac12}$, $\boldsymbol{K}_h^0$, for any $n\geqslant 0$, find $\boldsymbol{E}_h^{n+1}$, $\boldsymbol{H}_h^{n+\frac32}$, $\boldsymbol{J}_h^{n+\frac32}$, $\boldsymbol{K}_h^{n+1}\in\boldsymbol{V}_h$ such that

$$\epsilon_0\int_{T_i}\frac{\boldsymbol{E}_h^{n+1}-\boldsymbol{E}_h^n}{\tau}\cdot\boldsymbol{u}_h-\int_{T_i}\boldsymbol{H}_h^{n+\frac12}\cdot\nabla\times\boldsymbol{u}_h-\sum_{K\in\nu_i}\int_{a_{ik}}\boldsymbol{u}_h\cdot\boldsymbol{n}_{ik}\times\left\{\left\{\boldsymbol{H}_h^{n+\frac12}\right\}\right\}_{ik}+\int_{T_i}\boldsymbol{J}_h^{n+\frac12}\cdot\boldsymbol{u}_h=0,\tag{22}$$

$$\mu_0\int_{T_i}\frac{\boldsymbol{H}_h^{n+\frac32}-\boldsymbol{H}_h^{n+\frac12}}{\tau}\cdot\boldsymbol{v}_h+\int_{T_i}\boldsymbol{E}_h^{n+1}\cdot\nabla\times\boldsymbol{v}_h+\sum_{K\in\nu_i}\int_{a_{ik}}\boldsymbol{v}_h\cdot\boldsymbol{n}_{ik}\times\left\{\left\{\boldsymbol{E}_h^{n+1}\right\}\right\}_{ik}+\int_{T_i}\boldsymbol{K}_h^{n+1}\cdot\boldsymbol{v}_h=0,\tag{23}$$

$$\frac{1}{\epsilon_0\omega_{pe}^2}\int_{T_i}\frac{\boldsymbol{J}_h^{n+\frac32}-\boldsymbol{J}_h^{n+\frac12}}{\tau}\cdot\boldsymbol{\phi}_h+\frac{\Gamma_e}{\epsilon_0\omega_{pe}^2}\int_{T_i}\frac{\boldsymbol{J}_h^{n+\frac32}+\boldsymbol{J}_h^{n+\frac12}}{2}\cdot\boldsymbol{\phi}_h-\int_{T_i}\boldsymbol{E}_h^{n+1}\cdot\boldsymbol{\phi}_h=0,\tag{24}$$

$$\frac{1}{\mu_0\omega_{pm}^2}\int_{T_i}\frac{\boldsymbol{K}_h^{n+1}-\boldsymbol{K}_h^n}{\tau}\cdot\boldsymbol{\psi}_h+\frac{\Gamma_m}{\mu_0\omega_{pm}^2}\int_{T_i}\frac{\boldsymbol{K}_h^{n+1}+\boldsymbol{K}_h^n}{2}\cdot\boldsymbol{\psi}_h-\int_{T_i}\boldsymbol{H}_h^{n+\frac12}\cdot\boldsymbol{\psi}_h=0,\tag{25}$$

hold true for any $\boldsymbol{u}_h,\boldsymbol{v}_h,\boldsymbol{\phi}_h,\boldsymbol{\psi}_h\in\boldsymbol{V}_h$, and any element $T_i\in T_h$.

Remark 2.1. We like to remark that the current scheme (22)–(25) is simpler but more efficient than the leap-frog scheme developed in our early work [17]. Compared to (8)–(9) of [17], use of central flux in (22)–(23) makes the implementation simpler and more efficient, since we only need to invert the mass matrix, i.e., no extra matrices will be contributed to coefficient matrix. Moreover, since central flux decouples the $\boldsymbol{E}$ and $\boldsymbol{H}$ fields, the stability and error estimate analysis for this new scheme can be done more succinctly. Though numerical results with the upwind flux [17] achieve optimal convergence rate $O(h^{k+1})$, both schemes have the same theoretical error estimate $O(\tau^2+h^k)$.

Denote $c_v=\frac{1}{\sqrt{\epsilon_0\mu_0}}$ for the wave propagation speed in vacuum, $c_{inv}>0$ for the constant in the standard inverse estimate

$$\|\nabla\times\boldsymbol{\phi}_h\|_0\leqslant c_{inv}h^{-1}\|\boldsymbol{\phi}_h\|_0\quad\forall\boldsymbol{\phi}_h\in\boldsymbol{V}_h,\tag{26}$$

and $c_{tr}>0$ for the constant in the standard trace inequality

$$\|\boldsymbol{\phi}_h\|_{0,\partial\Omega}\leqslant c_{tr}h^{-1/2}\|\boldsymbol{\phi}_h\|_{0,\Omega}\quad\forall\boldsymbol{\phi}_h\in\boldsymbol{V}_h.\tag{27}$$

Theorem 2.3. *Under the CFL condition*

$$\tau \leqslant \min\left\{\frac{h}{2c_v c_{inv}}, \frac{h}{c_{tr}^2 c_v}, \frac{1}{\sqrt{2}\omega_{pe}}, \frac{1}{\sqrt{2}\omega_{pm}}\right\}, \tag{28}$$

the solution $(\boldsymbol{E}_h^{N+1}, \boldsymbol{H}_h^{N+\frac{3}{2}}, \boldsymbol{J}_h^{N+\frac{3}{2}}, \boldsymbol{K}_h^{N+1})$ *of (22)–(25) satisfies the following stability: For any* $N \geqslant 0$,

$$\begin{aligned}
&\epsilon_0 \|\boldsymbol{E}_h^{N+1}\|_{0,\Omega}^2 + \mu_0 \|\boldsymbol{H}_h^{N+\frac{3}{2}}\|_{0,\Omega}^2 + \frac{1}{\epsilon_0\omega_{pe}^2}\|\boldsymbol{J}_h^{N+\frac{3}{2}}\|_{0,\Omega}^2 + \frac{1}{\mu_0\omega_{pm}^2}\|\boldsymbol{K}_h^{N+1}\|_{0,\Omega}^2 \\
&\quad \leqslant C\left[\epsilon_0 \|\boldsymbol{E}_h^0\|_{0,\Omega}^2 + \mu_0 \|\boldsymbol{H}_h^{\frac{1}{2}}\|_{0,\Omega}^2 + \frac{1}{\epsilon_0\omega_{pe}^2}\|\boldsymbol{J}_h^{\frac{1}{2}}\|_{0,\Omega}^2 + \frac{1}{\mu_0\omega_{pm}^2}\|\boldsymbol{K}_h^0\|_{0,\Omega}^2\right]
\end{aligned} \tag{29}$$

holds true, where the constant $C > 0$ *is independent of* h, τ, N *and* T.

Proof. Choosing $\boldsymbol{u}_h = \frac{\tau}{2}(\boldsymbol{E}_i^{n+1} + \boldsymbol{E}_i^n)$, $\boldsymbol{v}_h = \frac{\tau}{2}(\boldsymbol{H}_i^{n+\frac{3}{2}} + \boldsymbol{H}_i^{n+\frac{1}{2}})$, $\boldsymbol{\phi}_h = \frac{\tau}{2}(\boldsymbol{J}_i^{n+\frac{3}{2}} + \boldsymbol{J}_i^{n+\frac{1}{2}})$, $\boldsymbol{\psi}_h = \frac{\tau}{2}(\boldsymbol{K}_i^{n+1} + \boldsymbol{K}_i^n)$ in (22)–(25), respectively, we obtain

$$\begin{aligned}
&\frac{\epsilon_0}{2}\left(\|\boldsymbol{E}_i^{n+1}\|_{0,T_i}^2 - \|\boldsymbol{E}_i^n\|_{0,T_i}^2\right) + \frac{\mu_0}{2}\left(\|\boldsymbol{H}_i^{n+\frac{3}{2}}\|_{0,T_i}^2 - \|\boldsymbol{H}_i^{n+\frac{1}{2}}\|_{0,T_i}^2\right) \\
&\quad + \frac{1}{2\epsilon_0\omega_{pe}^2}\left(\|\boldsymbol{J}_i^{n+\frac{3}{2}}\|_{0,T_i}^2 - \|\boldsymbol{J}_i^{n+\frac{1}{2}}\|_{0,T_i}^2\right) + \frac{1}{2\mu_0\omega_{pm}^2}\left(\|\boldsymbol{K}_i^{n+1}\|_{0,T_i}^2 - \|\boldsymbol{K}_i^n\|_{0,T_i}^2\right) \\
&\quad + \frac{\tau\Gamma_e}{\epsilon_0\omega_{pe}^2}\left\|\frac{\boldsymbol{J}_i^{n+\frac{3}{2}} + \boldsymbol{J}_i^{n+\frac{1}{2}}}{2}\right\|_{0,T_i}^2 + \frac{\tau\Gamma_m}{\mu_0\omega_{pm}^2}\left\|\frac{\boldsymbol{K}_i^{n+1} + \boldsymbol{K}_i^n}{2}\right\|_{0,T_i}^2 \\
&= \frac{\tau}{2}\left[\int_{T_i} \boldsymbol{H}_i^{n+\frac{1}{2}} \cdot \nabla \times \left(\boldsymbol{E}_i^{n+1} + \boldsymbol{E}_i^n\right) - \int_{T_i} \boldsymbol{E}_i^{n+1} \cdot \nabla \times \left(\boldsymbol{H}_i^{n+\frac{3}{2}} + \boldsymbol{H}_i^{n+\frac{1}{2}}\right)\right] \\
&\quad + \sum_{K\in\nu_i}\int_{a_{ik}} \frac{\tau}{2}\left(\boldsymbol{E}_i^{n+1} + \boldsymbol{E}_i^n\right)\cdot\boldsymbol{n}_{ik} \times \left\{\left\{\boldsymbol{H}_h^{n+\frac{1}{2}}\right\}\right\}_{ik} - \sum_{K\in\nu_i}\int_{a_{ik}} \frac{\tau}{2}\left(\boldsymbol{H}_i^{n+\frac{3}{2}} + \boldsymbol{H}_i^{n+\frac{1}{2}}\right)\cdot\boldsymbol{n}_{ik} \times \left\{\left\{\boldsymbol{E}_h^{n+1}\right\}\right\}_{ik} \\
&\quad - \int_{T_i} \boldsymbol{J}_i^{n+\frac{1}{2}} \cdot \frac{\tau}{2}\left(\boldsymbol{E}_i^{n+1} + \boldsymbol{E}_i^n\right) + \int_{T_i} \boldsymbol{E}_i^{n+1} \cdot \frac{\tau}{2}\left(\boldsymbol{J}_i^{n+\frac{3}{2}} + \boldsymbol{J}_i^{n+\frac{1}{2}}\right) \\
&\quad - \int_{T_i} \boldsymbol{K}_i^{n+1} \cdot \frac{\tau}{2}\left(\boldsymbol{H}_i^{n+\frac{3}{2}} + \boldsymbol{H}_i^{n+\frac{1}{2}}\right) + \int_{T_i} \boldsymbol{H}_i^{n+\frac{1}{2}} \cdot \frac{\tau}{2}\left(\boldsymbol{K}_i^{n+1} + \boldsymbol{K}_i^n\right).
\end{aligned} \tag{30}$$

Using the Stokes' formula, we have

$$\int_{T_i} \boldsymbol{H}_i^{n+\frac{1}{2}} \cdot \nabla \times \left(\boldsymbol{E}_i^{n+1} + \boldsymbol{E}_i^n\right) = \int_{T_i} \nabla \times \boldsymbol{H}_i^{n+\frac{1}{2}} \cdot \left(\boldsymbol{E}_i^{n+1} + \boldsymbol{E}_i^n\right) - \sum_{K\in\nu_i}\int_{a_{ik}} \left(\boldsymbol{E}_i^{n+1} + \boldsymbol{E}_i^n\right) \times \boldsymbol{H}_i^{n+\frac{1}{2}} \cdot \boldsymbol{n}_{ik}. \tag{31}$$

Adding all boundary integral terms in both (30) and (31), and using the average definition, we have

$$\begin{aligned}
sum_{1i} \equiv &\sum_{K\in\nu_i}\int_{a_{ik}} \frac{\tau}{2}\left(\boldsymbol{E}_h^{n+1} + \boldsymbol{E}_h^n\right)\cdot\boldsymbol{n}_{ik} \times \left\{\left\{\boldsymbol{H}_h^{n+\frac{1}{2}}\right\}\right\}_{ik} - \sum_{K\in\nu_i}\int_{a_{ik}} \frac{\tau}{2}\left(\boldsymbol{H}_h^{n+\frac{3}{2}} + \boldsymbol{H}_h^{n+\frac{1}{2}}\right)\cdot\boldsymbol{n}_{ik} \times \left\{\left\{\boldsymbol{E}_h^{n+1}\right\}\right\}_{ik} \\
&- \frac{\tau}{2}\sum_{K\in\nu_i}\int_{a_{ik}} \left(\boldsymbol{E}_i^{n+1} + \boldsymbol{E}_i^n\right) \times \boldsymbol{H}_i^{n+\frac{1}{2}} \cdot \boldsymbol{n}_{ik} \\
= &-\frac{\tau}{4}\sum_{K\in\nu_i}\int_{a_{ik}} \left[\left(\boldsymbol{E}_i^{n+1} + \boldsymbol{E}_i^n\right) \times \left(\boldsymbol{H}_i^{n+\frac{1}{2}} + \boldsymbol{H}_k^{n+\frac{1}{2}}\right) - \left(\boldsymbol{H}_i^{n+\frac{3}{2}} + \boldsymbol{H}_i^{n+\frac{1}{2}}\right) \times \left(\boldsymbol{E}_i^{n+1} + \boldsymbol{E}_k^{n+1}\right)\right. \\
&\left. - 2\left(\boldsymbol{E}_i^{n+1} + \boldsymbol{E}_i^n\right) \times \boldsymbol{H}_i^{n+\frac{1}{2}}\right] \cdot \boldsymbol{n}_{ik} \\
= &-\frac{\tau}{4}\sum_{K\in\nu_i}\int_{a_{ik}} \left[\boldsymbol{E}_i^n \times \boldsymbol{H}_k^{n+\frac{1}{2}} - \boldsymbol{E}_i^n \times \boldsymbol{H}_i^{n+\frac{1}{2}} + \boldsymbol{E}_i^{n+1} \times \boldsymbol{H}_i^{n+\frac{3}{2}}\right. \\
&\left. + \boldsymbol{E}_k^{n+1} \times \boldsymbol{H}_i^{n+\frac{1}{2}} + \boldsymbol{E}_i^{n+1} \times \boldsymbol{H}_k^{n+\frac{1}{2}} + \boldsymbol{E}_k^{n+1} \times \boldsymbol{H}_i^{n+\frac{3}{2}}\right] \cdot \boldsymbol{n}_{ik}.
\end{aligned} \tag{32}$$

Summing up (32) over all elements and using the jump definition, we have

$$\sum_{i=1}^{N_T} sum_{1i} = \frac{\tau}{4}\sum_{i=1}^{N_T}\sum_{K\in\nu_i}\int_{a_{ik}} \left(\boldsymbol{E}_i^{n+1}\times\left[\left[\boldsymbol{H}_h^{n+\frac{3}{2}}\right]\right]_{ik} - \boldsymbol{E}_i^{n}\times\left[\left[\boldsymbol{H}_h^{n+\frac{1}{2}}\right]\right]_{ik}\right)\cdot\boldsymbol{n}_{ik}. \tag{33}$$

It is easy to see that we have the following identities:

$$\begin{aligned}
&\frac{\tau}{2}\int_{T_i}\left[\nabla\times\boldsymbol{H}_i^{n+\frac{1}{2}}\cdot\left(\boldsymbol{E}_i^{n+1}+\boldsymbol{E}_i^{n}\right) - \boldsymbol{E}_i^{n+1}\cdot\nabla\times\left(\boldsymbol{H}_i^{n+\frac{3}{2}}+\boldsymbol{H}_i^{n+\frac{1}{2}}\right)\right]\\
&\quad= \frac{\tau}{2}\int_{T_i}\left[\boldsymbol{E}_i^{n}\cdot\nabla\times\boldsymbol{H}_i^{n+\frac{1}{2}} - \boldsymbol{E}_i^{n+1}\cdot\nabla\times\boldsymbol{H}_i^{n+\frac{3}{2}}\right],
\end{aligned} \tag{34}$$

$$\begin{aligned}
&\int_{T_i}\boldsymbol{E}_i^{n+1}\cdot\frac{\tau}{2}\left(\boldsymbol{J}_i^{n+\frac{3}{2}}+\boldsymbol{J}_i^{n+\frac{1}{2}}\right) - \int_{T_i}\boldsymbol{J}_i^{n+\frac{1}{2}}\cdot\frac{\tau}{2}\left(\boldsymbol{E}_i^{n+1}+\boldsymbol{E}_i^{n}\right)\\
&\quad= \frac{\tau}{2}\int_{T_i}\left(\boldsymbol{E}_i^{n+1}\cdot\boldsymbol{J}_i^{n+\frac{3}{2}} - \boldsymbol{E}_i^{n}\cdot\boldsymbol{J}_i^{n+\frac{1}{2}}\right),
\end{aligned} \tag{35}$$

and

$$\int_{T_i}\boldsymbol{H}_i^{n+\frac{1}{2}}\cdot\frac{\tau}{2}\left(\boldsymbol{K}_i^{n+1}+\boldsymbol{K}_i^{n}\right) - \int_{T_i}\boldsymbol{K}_i^{n+1}\cdot\frac{\tau}{2}\left(\boldsymbol{H}_i^{n+\frac{3}{2}}+\boldsymbol{H}_i^{n+\frac{1}{2}}\right) = \frac{\tau}{2}\int_{T_i}\left(\boldsymbol{H}_i^{n+\frac{1}{2}}\cdot\boldsymbol{K}_i^{n} - \boldsymbol{H}_i^{n+\frac{3}{2}}\cdot\boldsymbol{K}_i^{n+1}\right). \tag{36}$$

Summing up (30) first over all elements of Ω and then from $n=0$ to $n=N$, and using the identities (33)–(36), we have

$$\begin{aligned}
&\frac{\epsilon_0}{2}\left(\left\|\boldsymbol{E}_h^{N+1}\right\|_{0,\Omega}^2 - \left\|\boldsymbol{E}_h^{0}\right\|_{0,\Omega}^2\right) + \frac{\mu_0}{2}\left(\left\|\boldsymbol{H}_h^{N+\frac{3}{2}}\right\|_{0,\Omega}^2 - \left\|\boldsymbol{H}_h^{\frac{1}{2}}\right\|_{0,\Omega}^2\right)\\
&\quad+\frac{1}{2\epsilon_0\omega_{pe}^2}\left(\left\|\boldsymbol{J}_h^{N+\frac{3}{2}}\right\|_{0,\Omega}^2 - \left\|\boldsymbol{J}_h^{\frac{1}{2}}\right\|_{0,\Omega}^2\right) + \frac{1}{2\mu_0\omega_{pm}^2}\left(\left\|\boldsymbol{K}_h^{N+1}\right\|_{0,\Omega}^2 - \left\|\boldsymbol{K}_h^{0}\right\|_{0,\Omega}^2\right)\\
&\leqslant \frac{\tau}{4}\sum_{i=1}^{N_T}\sum_{K\in\nu_i}\int_{a_{ik}}\left(\boldsymbol{E}_i^{N+1}\times\left[\left[\boldsymbol{H}_h^{N+\frac{3}{2}}\right]\right]_{ik} - \boldsymbol{E}_i^{0}\times\left[\left[\boldsymbol{H}_h^{\frac{1}{2}}\right]\right]_{ik}\right)\cdot\boldsymbol{n}_{ik} + \frac{\tau}{2}\int_{\Omega}\left[\boldsymbol{E}_h^{0}\cdot\nabla\times\boldsymbol{H}_h^{\frac{1}{2}} - \boldsymbol{E}_h^{N+1}\cdot\nabla\times\boldsymbol{H}_h^{N+\frac{3}{2}}\right]\\
&\quad+\frac{\tau}{2}\int_{\Omega}\left(\boldsymbol{E}_h^{N+1}\cdot\boldsymbol{J}_h^{N+\frac{3}{2}} - \boldsymbol{E}_h^{0}\cdot\boldsymbol{J}_h^{\frac{1}{2}}\right) + \frac{\tau}{2}\int_{\Omega}\left(\boldsymbol{H}_h^{\frac{1}{2}}\cdot\boldsymbol{K}_h^{0} - \boldsymbol{H}_h^{N+\frac{3}{2}}\cdot\boldsymbol{K}_h^{N+1}\right).
\end{aligned} \tag{37}$$

Now we try to bound the right hand side terms of (37) by the corresponding terms on the left hand side. Below we will constantly use the standard arithmetic–geometric mean (AGM) inequality:

$$(a,b)\leqslant\delta\|a\|_0^2 + \frac{1}{4\delta}\|b\|_0^2. \tag{38}$$

Using the definition c_v, the inverse inequality (26), and the AGM inequality (38), we have

$$\begin{aligned}
\frac{\tau}{2}\int_{\Omega}\boldsymbol{E}_h^{N+1}\cdot\nabla\times\boldsymbol{H}_h^{N+\frac{3}{2}} &= \frac{\tau c_v}{2}\int_{\Omega}\sqrt{\epsilon_0}\boldsymbol{E}_h^{N+1}\cdot\sqrt{\mu_0}\nabla\times\boldsymbol{H}_h^{N+\frac{3}{2}}\\
&\leqslant \delta_1\epsilon_0\left\|\boldsymbol{E}_h^{N+1}\right\|_{0,\Omega}^2 + \frac{1}{4\delta_1}\cdot\left(\frac{\tau c_v c_{inv}h^{-1}}{2}\right)^2\cdot\mu_0\left\|\boldsymbol{H}_h^{N+\frac{3}{2}}\right\|_{0,\Omega}^2.
\end{aligned} \tag{39}$$

Similarly, we can obtain

$$\begin{aligned}
\frac{\tau}{2}\int_{\Omega}\boldsymbol{E}_h^{N+1}\cdot\boldsymbol{J}_h^{N+\frac{3}{2}} &= \frac{\tau\omega_{pe}}{2}\int_{\Omega}\sqrt{\epsilon_0}\boldsymbol{E}_h^{N+1}\cdot\frac{1}{\sqrt{\epsilon_0}\omega_{pe}}\boldsymbol{J}_h^{N+\frac{3}{2}}\\
&\leqslant \delta_2\epsilon_0\left\|\boldsymbol{E}_h^{N+1}\right\|_{0,\Omega}^2 + \frac{1}{4\delta_2}\cdot\left(\frac{\tau\omega_{pe}}{2}\right)^2\cdot\frac{1}{\epsilon_0\omega_{pe}^2}\left\|\boldsymbol{J}_h^{N+\frac{3}{2}}\right\|_{0,\Omega}^2,
\end{aligned} \tag{40}$$

and

$$\frac{\tau}{2}\int_{\Omega}\boldsymbol{H}_h^{N+\frac{3}{2}}\cdot\boldsymbol{K}_h^{N+1}=\frac{\tau\omega_{pm}}{2}\int_{\Omega}\sqrt{\mu_0}\boldsymbol{H}_h^{N+\frac{3}{2}}\cdot\frac{1}{\sqrt{\mu_0}\omega_{pm}}\boldsymbol{K}_h^{N+1}$$
$$\leqslant\delta_3\mu_0\big\|\boldsymbol{H}_h^{N+\frac{3}{2}}\big\|_{0,\Omega}^2+\frac{1}{4\delta_3}\cdot\left(\frac{\tau\omega_{pm}}{2}\right)^2\cdot\frac{1}{\mu_0\omega_{pm}^2}\big\|\boldsymbol{K}_h^{N+1}\big\|_{0,\Omega}^2. \tag{41}$$

Finally, using the trace inequality (27) and the AGM inequality (38), we have

$$\frac{\tau}{4}\sum_{i=1}^{N_T}\sum_{K\in\nu_i}\int_{a_{ik}}\big(\boldsymbol{E}_i^{N+1}\times\big[\big[\boldsymbol{H}_h^{N+\frac{3}{2}}\big]\big]_{ik}\big)\cdot\boldsymbol{n}_{ik}$$
$$\leqslant\frac{\tau}{4}\sum_{i=1}^{N_T}c_{tr}h^{-1/2}\big\|\boldsymbol{E}_i^{N+1}\big\|_{0,T_i}\cdot c_{tr}h^{-1/2}\big\|\boldsymbol{H}_h^{N+\frac{3}{2}}\big\|_{0,T_i}$$
$$=\frac{\tau}{4}\cdot c_{tr}^2h^{-1}c_v\sum_{i=1}^{N_T}\sqrt{\epsilon_0}\big\|\boldsymbol{E}_i^{N+1}\big\|_{0,T_i}\cdot\sqrt{\mu_0}\big\|\boldsymbol{H}_h^{N+\frac{3}{2}}\big\|_{0,T_i}$$
$$\leqslant\delta_4\epsilon\big\|\boldsymbol{E}_h^{N+1}\big\|_{0,\Omega}^2+\frac{1}{4\delta_4}\cdot\left(\frac{\tau c_{tr}^2c_vh^{-1}}{4}\right)^2\cdot\mu_0\big\|\boldsymbol{H}_h^{N+\frac{3}{2}}\big\|_{0,\Omega}^2. \tag{42}$$

First choosing δ_i $(i=1,2,3,4)$ small enough, then choosing τ satisfying the CFL condition $\tau\leqslant Ch$, we can obtain the following stability

$$\epsilon_0\big\|\boldsymbol{E}_h^{N+1}\big\|_{0,\Omega}^2+\mu_0\big\|\boldsymbol{H}_h^{N+\frac{3}{2}}\big\|_{0,\Omega}^2+\frac{1}{\epsilon_0\omega_{pe}^2}\big\|\boldsymbol{J}_h^{N+\frac{3}{2}}\big\|_{0,\Omega}^2+\frac{1}{\mu_0\omega_{pm}^2}\big\|\boldsymbol{K}_h^{N+1}\big\|_{0,\Omega}^2$$
$$\leqslant C\left[\epsilon_0\big\|\boldsymbol{E}_h^0\big\|_{0,\Omega}^2+\mu_0\big\|\boldsymbol{H}_h^{\frac{1}{2}}\big\|_{0,\Omega}^2+\frac{1}{\epsilon_0\omega_{pe}^2}\big\|\boldsymbol{J}_h^{\frac{1}{2}}\big\|_{0,\Omega}^2+\frac{1}{\mu_0\omega_{pm}^2}\big\|\boldsymbol{K}_h^0\big\|_{0,\Omega}^2\right].$$

A simple choice is $\delta_1=\delta_2=\delta_3=\delta_4=\frac{1}{8}$, and

$$\big(\tau c_vc_{inv}h^{-1}\big)^2\leqslant\frac{1}{4},\qquad\big(\tau c_{tr}^2c_vh^{-1}\big)^2\leqslant1,\qquad(\tau\omega_{pe})^2\leqslant\frac{1}{2},\qquad(\tau\omega_{pm})^2\leqslant\frac{1}{2},$$

which leads to a choice of τ as (28). This completes our proof. □

Note that the above stability result is obtained without using the discrete Gronwall inequality often seen in analyzing time-dependent problems. Finally, we like to point out the following error estimate for our scheme (22)–(25).

Theorem 2.4. *Let $(\boldsymbol{E}^{n+1},\boldsymbol{H}^{n+\frac{3}{2}},\boldsymbol{J}^{n+\frac{3}{2}},\boldsymbol{K}^{n+1})$ and $(\boldsymbol{E}_h^{n+1},\boldsymbol{H}_h^{n+\frac{3}{2}},\boldsymbol{J}_h^{n+\frac{3}{2}},\boldsymbol{K}_h^{n+1})$ be the solutions of (1)–(4) and (22)–(25). at time t_{n+1} or $t_{n+\frac{3}{2}}$. Then under the CFL condition (28), there exists a constant $C>0$, independent of τ and h, such that for any $n\geqslant0$ we have*

$$\max_{n\geqslant0}\big(\big\|\boldsymbol{E}_h^{n+1}-\boldsymbol{E}^{n+1}\big\|_{0,\Omega}+\big\|\boldsymbol{H}_h^{n+\frac{3}{2}}-\boldsymbol{H}^{n+\frac{3}{2}}\big\|_{0,\Omega}+\big\|\boldsymbol{J}_h^{n+\frac{3}{2}}-\boldsymbol{J}^{n+\frac{3}{2}}\big\|_{0,\Omega}+\big\|\boldsymbol{K}_h^{n+1}-\boldsymbol{K}^{n+1}\big\|_{0,\Omega}\big)$$
$$\leqslant C\big(\tau^2+h^k\big)+C\big(\big\|\boldsymbol{E}_h^0-\boldsymbol{E}^0\big\|_{0,\Omega}+\big\|\boldsymbol{H}_h^{\frac{1}{2}}-\boldsymbol{H}^{\frac{1}{2}}\big\|_{0,\Omega}+\big\|\boldsymbol{J}_h^{\frac{1}{2}}-\boldsymbol{J}^{\frac{1}{2}}\big\|_{0,\Omega}+\big\|\boldsymbol{K}_h^0-\boldsymbol{K}^0\big\|_{0,\Omega}\big), \tag{43}$$

where $k\geqslant1$ is the order of basis function in the space $\boldsymbol{V}_h$.

Proof. Integrating (8) and (11) from t_n to t_{n+1}, and (9) and (10) from $t_{n+\frac{1}{2}}$ to $t_{n+\frac{3}{2}}$, we have

$$\epsilon_0\int_{T_i}\frac{\boldsymbol{E}^{n+1}-\boldsymbol{E}^n}{\tau}\cdot\boldsymbol{u}-\int_{T_i}\left(\frac{1}{\tau}\int_{t_n}^{t_{n+1}}\boldsymbol{H}\right)\cdot\nabla\times\boldsymbol{u}-\int_{\partial T_i}\boldsymbol{n}_i\times\left(\frac{1}{\tau}\int_{t_n}^{t_{n+1}}\boldsymbol{H}\right)\cdot\boldsymbol{u}+\int_{T_i}\left(\frac{1}{\tau}\int_{t_n}^{t_{n+1}}\boldsymbol{J}\right)\cdot\boldsymbol{u}=0, \tag{44}$$
$$\mu_0\int_{T_i}\frac{\boldsymbol{H}^{n+\frac{3}{2}}-\boldsymbol{H}^{n+\frac{1}{2}}}{\tau}\cdot\boldsymbol{v}+\int_{T_i}\left(\frac{1}{\tau}\int_{t_{n+\frac{1}{2}}}^{t_{n+\frac{3}{2}}}\boldsymbol{E}\right)\cdot\nabla\times\boldsymbol{v}+\int_{\partial T_i}\boldsymbol{n}_i\times\left(\frac{1}{\tau}\int_{t_{n+\frac{1}{2}}}^{t_{n+\frac{3}{2}}}\boldsymbol{E}\right)\cdot\boldsymbol{v}+\int_{T_i}\left(\frac{1}{\tau}\int_{t_{n+\frac{1}{2}}}^{t_{n+\frac{3}{2}}}\boldsymbol{K}\right)\cdot\boldsymbol{v}=0,$$

$$\frac{1}{\epsilon_0\omega_{pe}^2}\int_{T_i}\frac{\boldsymbol{J}^{n+\frac{3}{2}}-\boldsymbol{J}^{n+\frac{1}{2}}}{\tau}\cdot\boldsymbol{\phi}+\frac{\Gamma_e}{\epsilon_0\omega_{pe}^2}\int_{T_i}\left(\frac{1}{\tau}\int_{t_{n+\frac{1}{2}}}^{t_{n+\frac{3}{2}}}\boldsymbol{J}\right)\cdot\boldsymbol{\phi}=\int_{T_i}\left(\frac{1}{\tau}\int_{t_{n+\frac{1}{2}}}^{t_{n+\frac{3}{2}}}\boldsymbol{E}\right)\cdot\boldsymbol{\phi}, \tag{45}$$

$$\frac{1}{\mu_0\omega_{pm}^2}\int_{T_i}\frac{\boldsymbol{K}^{n+1}-\boldsymbol{K}^{n}}{\tau}\cdot\boldsymbol{\psi}+\frac{\Gamma_m}{\mu_0\omega_{pm}^2}\int_{T_i}\left(\frac{1}{\tau}\int_{t_n}^{t_{n+1}}\boldsymbol{K}\right)\cdot\boldsymbol{\psi}=\int_{T_i}\left(\frac{1}{\tau}\int_{t_n}^{t_{n+1}}\boldsymbol{H}\right)\cdot\boldsymbol{\psi}. \tag{46}$$

Denote $\tilde{\boldsymbol{W}}_h=\Pi_2(\boldsymbol{W})-\boldsymbol{W}_h$ and $\overline{\boldsymbol{W}}_h=\Pi_2(\boldsymbol{W})-\boldsymbol{W}$ for $\boldsymbol{W}=\boldsymbol{E},\boldsymbol{H},\boldsymbol{J},\boldsymbol{K}$. Then we can obtain error equations by subtracting (22)–(25) from (44)–(46) with $\boldsymbol{u}=\boldsymbol{u}_h$, $\boldsymbol{v}=\boldsymbol{v}_h$, $\boldsymbol{\phi}=\boldsymbol{\phi}_h$ and $\boldsymbol{\psi}=\boldsymbol{\psi}_h$:

$$\begin{aligned}
&\epsilon_0\int_{T_i}\frac{\tilde{\boldsymbol{E}}_h^{n+1}-\tilde{\boldsymbol{E}}_h^{n}}{\tau}\cdot\boldsymbol{u}_h-\int_{T_i}\tilde{\boldsymbol{H}}_h^{n+\frac{1}{2}}\cdot\nabla\times\boldsymbol{u}_h-\sum_{K\in\nu_i}\int_{a_{ik}}\boldsymbol{u}_h\cdot\boldsymbol{n}_{ik}\times\left\{\left\{\tilde{\boldsymbol{H}}_h^{n+\frac{1}{2}}\right\}\right\}_{ik}+\int_{T_i}\tilde{\boldsymbol{J}}_h^{n+\frac{1}{2}}\cdot\boldsymbol{u}_h\\
&=-\sum_{K\in\nu_i}\int_{a_{ik}}\boldsymbol{u}_h\cdot\boldsymbol{n}_{ik}\times\left(\left\{\left\{\overline{\boldsymbol{H}}_h^{n+\frac{1}{2}}\right\}\right\}_{ik}+\boldsymbol{H}^{n+\frac{1}{2}}-\frac{1}{\tau}\int_{t_n}^{t_{n+1}}\boldsymbol{H}\right)\\
&\quad-\int_{T_i}\left(\boldsymbol{H}^{n+\frac{1}{2}}-\frac{1}{\tau}\int_{t_n}^{t_{n+1}}\boldsymbol{H}\right)\cdot\nabla\times\boldsymbol{u}_h+\int_{T_i}\left(\boldsymbol{J}^{n+\frac{1}{2}}-\frac{1}{\tau}\int_{t_n}^{t_{n+1}}\boldsymbol{J}\right)\cdot\boldsymbol{u}_h,
\end{aligned} \tag{47}$$

$$\begin{aligned}
&\mu_0\int_{T_i}\frac{\tilde{\boldsymbol{H}}_h^{n+\frac{3}{2}}-\tilde{\boldsymbol{H}}_h^{n+\frac{1}{2}}}{\tau}\cdot\boldsymbol{v}_h+\int_{T_i}\tilde{\boldsymbol{E}}_h^{n+1}\cdot\nabla\times\boldsymbol{v}_h+\sum_{K\in\nu_i}\int_{a_{ik}}\boldsymbol{v}_h\cdot\boldsymbol{n}_{ik}\times\left\{\left\{\tilde{\boldsymbol{E}}_h^{n+1}\right\}\right\}_{ik}+\int_{T_i}\tilde{\boldsymbol{K}}_h^{n+1}\cdot\boldsymbol{v}_h\\
&=\sum_{K\in\nu_i}\int_{a_{ik}}\boldsymbol{v}_h\cdot\boldsymbol{n}_{ik}\times\left(\left\{\left\{\overline{\boldsymbol{E}}_h^{n+1}\right\}\right\}_{ik}+\boldsymbol{E}^{n+1}-\frac{1}{\tau}\int_{t_{n+\frac{1}{2}}}^{t_{n+\frac{3}{2}}}\boldsymbol{E}\right)\\
&\quad+\int_{T_i}\left(\boldsymbol{E}^{n+1}-\frac{1}{\tau}\int_{t_{n+\frac{1}{2}}}^{t_{n+\frac{3}{2}}}\boldsymbol{E}\right)\cdot\nabla\times\boldsymbol{v}_h+\int_{T_i}\left(\boldsymbol{K}^{n+1}-\frac{1}{\tau}\int_{t_{n+\frac{1}{2}}}^{t_{n+\frac{3}{2}}}\boldsymbol{K}\right)\cdot\boldsymbol{v}_h,
\end{aligned} \tag{48}$$

$$\begin{aligned}
&\frac{1}{\epsilon_0\omega_{pe}^2}\int_{T_i}\frac{\tilde{\boldsymbol{J}}_h^{n+\frac{3}{2}}-\tilde{\boldsymbol{J}}_h^{n+\frac{1}{2}}}{\tau}\cdot\boldsymbol{\phi}_h+\frac{\Gamma_e}{\epsilon_0\omega_{pe}^2}\int_{T_i}\frac{\tilde{\boldsymbol{J}}_h^{n+\frac{3}{2}}+\tilde{\boldsymbol{J}}_h^{n+\frac{1}{2}}}{2}\cdot\boldsymbol{\phi}_h-\int_{T_i}\tilde{\boldsymbol{E}}_h^{n+1}\cdot\boldsymbol{\phi}_h\\
&=\frac{\Gamma_e}{\epsilon_0\omega_{pe}^2}\int_{T_i}\left(\frac{\boldsymbol{J}^{n+\frac{3}{2}}+\boldsymbol{J}^{n+\frac{1}{2}}}{2}-\frac{1}{\tau}\int_{t_{n+\frac{1}{2}}}^{t_{n+\frac{3}{2}}}\boldsymbol{J}\right)\cdot\boldsymbol{\phi}_h-\int_{T_i}\left(\boldsymbol{E}^{n+1}-\frac{1}{\tau}\int_{t_{n+\frac{1}{2}}}^{t_{n+\frac{3}{2}}}\boldsymbol{E}\right)\cdot\boldsymbol{\phi}_h,
\end{aligned} \tag{49}$$

$$\begin{aligned}
&\frac{1}{\mu_0\omega_{pm}^2}\int_{T_i}\frac{\tilde{\boldsymbol{K}}_h^{n+1}-\tilde{\boldsymbol{K}}_h^{n}}{\tau}\cdot\boldsymbol{\psi}_h+\frac{\Gamma_m}{\mu_0\omega_{pm}^2}\int_{T_i}\frac{\tilde{\boldsymbol{K}}_h^{n+1}+\tilde{\boldsymbol{K}}_h^{n}}{2}\cdot\boldsymbol{\psi}_h-\int_{T_i}\tilde{\boldsymbol{H}}_h^{n+\frac{1}{2}}\cdot\boldsymbol{\psi}_h\\
&=\frac{\Gamma_m}{\mu_0\omega_{pm}^2}\int_{T_i}\left(\frac{\boldsymbol{K}^{n+1}+\boldsymbol{K}^{n}}{2}-\frac{1}{\tau}\int_{t_n}^{t_{n+1}}\boldsymbol{K}\right)\cdot\boldsymbol{\psi}_h-\int_{T_i}\left(\boldsymbol{H}^{n+\frac{1}{2}}-\frac{1}{\tau}\int_{t_n}^{t_{n+1}}\boldsymbol{H}\right)\cdot\boldsymbol{\psi}_h.
\end{aligned} \tag{50}$$

The rest of the proof is similar to the stability proof carried out for Theorem 2.3, and is skipped due to the technicality. □

3. Extension of the DG method to the PML model

To model wave propagation in practice, we need to truncate an infinite physical domain to a bounded domain. To easily couple with our metamaterial Maxwell's equations (1)–(4), we choose a perfectly matched layer (PML) model developed

by Ziolkowski [26] in 1997. Following [26], the PML is assumed to enclose a cubical simulation domain in $\mathcal{R}^3$, and the complete PML governing equations for the corner region are given by [26, Eq. (B.4)]:

$$\frac{\partial \boldsymbol{E}}{\partial t} + D_1\boldsymbol{E} = \frac{1}{\epsilon_0}\nabla\times\boldsymbol{H} - \frac{1}{\epsilon_0}\boldsymbol{J}, \tag{51}$$

$$\frac{\partial \boldsymbol{J}}{\partial t} + D_2\boldsymbol{J} = \epsilon_0 D_3\boldsymbol{E}, \tag{52}$$

$$\frac{\partial \boldsymbol{H}}{\partial t} + D_1\boldsymbol{H} = -\frac{1}{\mu_0}\nabla\times\boldsymbol{E} - \frac{1}{\mu_0}\boldsymbol{K}, \tag{53}$$

$$\frac{\partial \boldsymbol{K}}{\partial t} + D_2\boldsymbol{K} = \mu_0 D_3\boldsymbol{H}, \tag{54}$$

where ϵ_0 and μ_0, $\boldsymbol{E}(\boldsymbol{x},t)$ and $\boldsymbol{H}(\boldsymbol{x},t)$, and $\boldsymbol{J}(\boldsymbol{x},t)$ and $\boldsymbol{K}(\boldsymbol{x},t)$ have the same meaning as given in the system (1)–(4). Moreover, D_1, D_2 and D_3 are 3×3 diagonal matrices given by $D_1 = \mathrm{diag}(\sigma_y+\sigma_z-\sigma_x, \sigma_z+\sigma_x-\sigma_y, \sigma_x+\sigma_y-\sigma_z)$, $D_2 = \mathrm{diag}(\sigma_x,\sigma_y,\sigma_z)$, $D_3 = \mathrm{diag}((\sigma_x-\sigma_y)(\sigma_x-\sigma_z), (\sigma_y-\sigma_x)(\sigma_y-\sigma_z), (\sigma_z-\sigma_x)(\sigma_z-\sigma_y))$. Here σ_x, σ_y and σ_z are nonnegative functions and represent the damping variations along the x, y and z directions, respectively. Note that the PML equations (51)–(54) should be modified accordingly at other regions. For example, in the face regions, only one normal direction has absorbing layers.

Note that the model (51)–(54) with $\epsilon_0 = \mu_0 = 1$ is the same as (5.12) of Turkel and Yefet [24], and is well-posed mathematically because it is a symmetric hyperbolic system (i.e., the standard Maxwell equations) plus lower-order terms [24, p. 545].

We like to remark that all the results in previous section can be extended easily to this PML model, but the proofs become more involved. For clarity, below we just briefly present the semi- and fully-discrete schemes for solving (51)–(54).

The semi-discrete DG method for (51)–(54): For any $\boldsymbol{u}_h, \boldsymbol{v}_h, \boldsymbol{\phi}_h, \boldsymbol{\psi}_h \in \boldsymbol{V}_h$, and any element $T_i \in T_h$, find $\boldsymbol{E}_h, \boldsymbol{H}_h, \boldsymbol{J}_h, \boldsymbol{K}_h \in C^1(0,T;\boldsymbol{V}_h)$ such that

$$\epsilon_0\int_{T_i}\frac{\partial \boldsymbol{E}_h}{\partial t}\cdot\boldsymbol{u}_h - \int_{T_i}\boldsymbol{H}_h\cdot\nabla\times\boldsymbol{u}_h - \sum_{K\in\nu_i}\int_{a_{ik}}\boldsymbol{u}_h\cdot\boldsymbol{n}_{ik}\times\{\{\boldsymbol{H}_h\}\}_{ik} + \int_{T_i}(\boldsymbol{J}_h+\epsilon_0 D_1\boldsymbol{E}_h)\cdot\boldsymbol{u}_h = 0, \tag{55}$$

$$\mu_0\int_{T_i}\frac{\partial \boldsymbol{H}_h}{\partial t}\cdot\boldsymbol{v}_h + \int_{T_i}\boldsymbol{E}_h\cdot\nabla\times\boldsymbol{v}_h + \sum_{K\in\nu_i}\int_{a_{ik}}\boldsymbol{v}_h\cdot\boldsymbol{n}_{ik}\times\{\{\boldsymbol{E}_h\}\}_{ik} + \int_{T_i}(\boldsymbol{K}_h+\mu_0 D_1\boldsymbol{H}_h)\cdot\boldsymbol{v}_h = 0, \tag{56}$$

$$\frac{1}{\epsilon_0}\int_{T_i}\frac{\partial \boldsymbol{J}_h}{\partial t}\cdot\boldsymbol{\phi}_h + \frac{1}{\epsilon_0}\int_{T_i}D_2\boldsymbol{J}_h\cdot\boldsymbol{\phi}_h = \int_{T_i}D_3\boldsymbol{E}_h\cdot\boldsymbol{\phi}_h, \tag{57}$$

$$\frac{1}{\mu_0}\int_{T_i}\frac{\partial \boldsymbol{K}_h}{\partial t}\cdot\boldsymbol{\psi}_h + \frac{1}{\mu_0}\int_{T_i}D_2\boldsymbol{K}_h\cdot\boldsymbol{\psi}_h = \int_{T_i}D_3\boldsymbol{H}_h\cdot\boldsymbol{\psi}_h, \tag{58}$$

hold true and are subject to the initial conditions (16).

Denote the semi-discrete energy $\mathcal{E}_h^{pml}$:

$$\mathcal{E}_h^{pml}(t) = \frac{1}{2}\left(\epsilon_0\|\boldsymbol{E}_h(t)\|_{0,\Omega}^2 + \mu_0\|\boldsymbol{H}_h(t)\|_{0,\Omega}^2 + \frac{1}{\epsilon_0}\|\boldsymbol{J}_h(t)\|_{0,\Omega}^2 + \frac{1}{\mu_0}\|\boldsymbol{K}_h(t)\|_{0,\Omega}^2\right). \tag{59}$$

Theorem 3.1. *The energy $\mathcal{E}_h^{pml}$ is bounded, i.e., $\mathcal{E}_h^{pml}(t) \leqslant C\mathcal{E}_h^{pml}(0)$ holds true for any $t\in[0,T]$, where the constant $C>0$ depends on T.*

Proof. Choosing $\boldsymbol{u}_h = \boldsymbol{E}_h, \boldsymbol{v}_h = \boldsymbol{H}_h, \boldsymbol{\phi}_h = \boldsymbol{J}_h, \boldsymbol{\psi}_h = \boldsymbol{K}_h$ in (55)–(58) and adding the results together over all element $T_i \in T_h$, we obtain

$$\begin{aligned}
&\frac{d}{dt}\mathcal{E}_h^{pml}(t) + \left\|\sqrt{\frac{D_2}{\epsilon_0}}\boldsymbol{J}_h(t)\right\|_{0,\Omega}^2 + \left\|\sqrt{\frac{D_2}{\mu_0}}\boldsymbol{K}_h(t)\right\|_{0,\Omega}^2 + \sum_i \mathcal{B}_i(\boldsymbol{E}_h,\boldsymbol{H}_h)\\
&\quad= -\int_\Omega \boldsymbol{J}_h\cdot\boldsymbol{E}_h - \int_\Omega \epsilon_0 D_1\boldsymbol{E}_h\cdot\boldsymbol{E}_h - \int_\Omega \boldsymbol{K}_h\cdot\boldsymbol{H}_h - \int_\Omega \mu_0 D_1\boldsymbol{H}_h\cdot\boldsymbol{H}_h + \int_\Omega D_3\boldsymbol{E}_h\cdot\boldsymbol{J}_h + \int_\Omega D_3\boldsymbol{H}_h\cdot\boldsymbol{K}_h\\
&\quad= \int_\Omega (D_3-I_3)\boldsymbol{H}_h\cdot\boldsymbol{K}_h + \int_\Omega (D_3-I_3)\boldsymbol{E}_h\cdot\boldsymbol{J}_h - \int_\Omega \epsilon_0 D_1\boldsymbol{E}_h\cdot\boldsymbol{E}_h - \int_\Omega \mu_0 D_1\boldsymbol{H}_h\cdot\boldsymbol{H}_h,
\end{aligned} \tag{60}$$

where we denote I_3 for the 3×3 identity matrix.

Using the fact that $\sum_i \mathcal{B}_i(\boldsymbol{E}_h, \boldsymbol{H}_h) = 0$, the Cauchy–Schwarz inequality to those right hand side terms of (60) with the boundedness of D_1 and D_3, and the Gronwall inequality, we complete the proof. □

Similar to the metamaterial model, we can construct the following leap-frog DG scheme: Given initial approximations of $\boldsymbol{E}_h^0$, $\boldsymbol{H}_h^{\frac{1}{2}}$, $\boldsymbol{J}_h^{\frac{1}{2}}$, $\boldsymbol{K}_h^0$, for any $n \geqslant 0$, find $\boldsymbol{E}_h^{n+1}, \boldsymbol{H}_h^{n+\frac{3}{2}}, \boldsymbol{J}_h^{n+\frac{3}{2}}, \boldsymbol{K}_h^{n+1} \in \boldsymbol{V}_h$ such that

$$\epsilon_0 \int_{T_i} \frac{\boldsymbol{E}_h^{n+1} - \boldsymbol{E}_h^n}{\tau} \cdot \boldsymbol{u}_h - \int_{T_i} \boldsymbol{H}_h^{n+\frac{1}{2}} \cdot \nabla \times \boldsymbol{u}_h - \sum_{K \in \nu_i} \int_{a_{ik}} \boldsymbol{u}_h \cdot \boldsymbol{n}_{ik} \times \left\{ \left\{ \boldsymbol{H}_h^{n+\frac{1}{2}} \right\} \right\}_{ik} + \int_{T_i} \left(\boldsymbol{J}_h^{n+\frac{1}{2}} + \frac{\epsilon_0 D_1}{2} \left(\boldsymbol{E}_h^{n+1} + \boldsymbol{E}_h^n \right) \right) \cdot \boldsymbol{u}_h = 0, \tag{61}$$

$$\mu_0 \int_{T_i} \frac{\boldsymbol{H}_h^{n+\frac{3}{2}} - \boldsymbol{H}_h^{n+\frac{1}{2}}}{\tau} \cdot \boldsymbol{v}_h + \int_{T_i} \boldsymbol{E}_h^{n+1} \cdot \nabla \times \boldsymbol{v}_h + \sum_{K \in \nu_i} \int_{a_{ik}} \boldsymbol{v}_h \cdot \boldsymbol{n}_{ik} \times \left\{ \left\{ \boldsymbol{E}_h^{n+1} \right\} \right\}_{ik} + \int_{T_i} \left(\boldsymbol{K}_h^{n+1} + \frac{\mu_0 D_1}{2} \left(\boldsymbol{H}_h^{n+\frac{3}{2}} + \boldsymbol{H}_h^{n+\frac{1}{2}} \right) \right) \cdot \boldsymbol{v}_h = 0, \tag{62}$$

$$\frac{1}{\epsilon_0} \int_{T_i} \frac{\boldsymbol{J}_h^{n+\frac{3}{2}} - \boldsymbol{J}_h^{n+\frac{1}{2}}}{\tau} \cdot \boldsymbol{\phi}_h + \int_{T_i} \frac{D_2}{2\epsilon_0} \left(\boldsymbol{J}_h^{n+\frac{3}{2}} + \boldsymbol{J}_h^{n+\frac{1}{2}} \right) \cdot \boldsymbol{\phi}_h = \int_{T_i} D_3 \boldsymbol{E}_h^{n+1} \cdot \boldsymbol{\phi}_h, \tag{63}$$

$$\frac{1}{\mu_0} \int_{T_i} \frac{\boldsymbol{K}_h^{n+1} - \boldsymbol{K}_h^n}{\tau} \cdot \boldsymbol{\psi}_h + \int_{T_i} \frac{D_2}{2\mu_0} \left(\boldsymbol{K}_h^{n+1} + \boldsymbol{K}_h^n \right) \cdot \boldsymbol{\psi}_h = \int_{T_i} D_3 \boldsymbol{H}_h^{n+\frac{1}{2}} \cdot \boldsymbol{\psi}_h, \tag{64}$$

hold true for any $\boldsymbol{u}_h, \boldsymbol{v}_h, \boldsymbol{\phi}_h, \boldsymbol{\psi}_h \in \boldsymbol{V}_h$, and any element $T_i \in T_h$.

In implementation, at each time step, we first solve (61) and (64) in parallel; then we solve (62) and (63) simultaneously.

4. Numerical results

Our implementation is based on the package *nudg* provided by [10]. Note that the theoretical results proved in previous sections hold true for both 3-D and 2-D cases. Here we show some interesting 2-D numerical results. All our tests are carried out using MATLAB R2011b running on Dell Precision WorkStation T7500 with 12 GB memory and 2.26 GHz Intel Xeon CPU.

4.1. Convergence rate test for the metamaterial model

Here we consider the 2-D transverse magnetic (TM) metamaterial model:

$$\frac{\partial H_x}{\partial t} = -\frac{\partial E_z}{\partial y} - K_x + g_x, \tag{65}$$

$$\frac{\partial H_y}{\partial t} = \frac{\partial E_z}{\partial x} - K_y + g_y, \tag{66}$$

$$\frac{\partial E_z}{\partial t} = \frac{\partial H_y}{\partial x} - \frac{\partial H_x}{\partial y} - J_z + f, \tag{67}$$

$$\frac{\partial J_z}{\partial t} = \omega_e^2 E_z - \Gamma_e J_z, \tag{68}$$

$$\frac{\partial K_x}{\partial t} = \omega_m^2 H_x - \Gamma_m K_x, \tag{69}$$

$$\frac{\partial K_y}{\partial t} = \omega_m^2 H_y - \Gamma_m K_y, \tag{70}$$

which is the 2-D version of (1)–(4) with $\epsilon_0 = \mu_0 = 1$ and added source terms g_x, g_y and f. In (65)–(70) the subscripts 'x, y' and 'z' denote the corresponding components in the x, y and z directions, respectively. Note that in TM model, the non-zero fields are H_x, H_y and E_z, and the induced currents K_x, K_y and J_z.

Table 1
Example 1. L_∞ and L_2 errors for magnetic field H_x with linear basis function and $\tau = 10^{-5}$ at 1000 time steps.

	$h = 1/5$	$h = 1/10$	Rates	$h = 1/20$	Rates	$h = 1/40$	Rates	$h = 1/80$	Rates
L_∞ errors	0.0171	0.0095	0.8480	0.0048	0.9849	0.0024	1.0	0.0012	1.0
L_2 errors	0.0046	0.0023	1.0	0.0011	1.0641	5.2752e–4	1.0602	2.1700e–4	1.2815
CPU(s)	17.19	17.65		29.61		33.72		44.05	

Table 2
Example 1. L_∞ and L_2 errors for magnetic field H_x with quadratic basis function and $\tau = 10^{-5}$ at 1000 time steps.

	$h = 1/5$	$h = 1/10$	Rates	$h = 1/20$	Rates	$h = 1/40$	Rates	$h = 1/80$	Rates
L_∞ errors	0.0039	9.7298e–4	2.0030	2.1093e–4	2.2056	4.7594e–5	2.1479	2.2728e–5	1.0663
L_2 errors	5.6795e–4	1.4231e–4	1.9967	3.3759e–5	2.0757	9.9027e–6	1.7694	7.6578e–6	0.3709
CPU(s)	18.76	19.60		30.38		33.48		58.35	

Example 1. To check the convergence rate for our scheme, we use the same exact solutions constructed in our previous work [14] (assuming that $\Gamma_m = \Gamma_e = \pi$, $\omega_m = \omega_e = \pi$ in (65)–(70)) on domain $\Omega = (0,1)^2$:

$$\boldsymbol{H} \equiv \begin{pmatrix} H_x \\ H_y \end{pmatrix} = \begin{pmatrix} \sin(\pi x)\cos(\pi y)\exp(-\pi t) \\ -\cos(\pi x)\sin(\pi y)\exp(-\pi t) \end{pmatrix},$$
$$E_z = \sin(\pi x)\sin(\pi y)\exp(-\pi t).$$

The corresponding magnetic and electric currents are

$$\boldsymbol{K} \equiv \begin{pmatrix} K_x \\ K_y \end{pmatrix} = \begin{pmatrix} \pi^2 t\sin(\pi x)\cos(\pi y)\exp(-\pi t) \\ -\pi^2 t\cos(\pi x)\sin(\pi y)\exp(-\pi t) \end{pmatrix},$$

and

$$J_z = \pi^2 t\sin(\pi x)\sin(\pi y)\exp(-\pi t),$$

respectively. The corresponding source terms are

$$f = \left(-3\pi + \pi^2 t\right)\sin(\pi x)\sin(\pi y)\exp(-\pi t),$$
$$g_x = \pi^2 t\sin(\pi x)\cos(\pi y)\exp(-\pi t),$$
$$g_y = -\pi^2 t\cos(\pi x)\sin(\pi y)\exp(-\pi t).$$

Notice that E_z satisfies the boundary condition $E_z = 0$ on $\partial\Omega$.

We solved this problem with various time steps τ and uniformly refined triangular meshes. In Table 1, we presented the numerical results obtained with linear basis function, $\tau = 10^{-5}$ running for 1000 time steps. Since the convergence rates are very similar for all the variables, we just presented H_x in Table 1, which shows clearly $O(h)$ rates in both L_∞ and L_2 norms.

In Table 2, we presented the numerical results obtained with quadratic basis function, $\tau = 10^{-5}$ running for 1000 time steps. Results of Table 2 show $O(h^2)$ rates in both L_∞ and L_2 norms, though the rates degenerate as the mesh becomes fine enough. The reason is that the solution error is dominated by the time error when the mesh is fine enough.

Example 2. To further check the convergence rate and our algorithmic implementation, we construct another exact solution for (65)–(70) on $\Omega = (0,1)^2$ by assuming that $\Gamma_m = \Gamma_e = 2\omega\pi$, $\omega_m = \omega_e = \omega\pi$:

$$\boldsymbol{H} \equiv \begin{pmatrix} H_x \\ H_y \end{pmatrix} = \begin{pmatrix} \sin(\omega\pi x)\cos(\omega\pi y)\exp(-\omega\pi t) \\ -\cos(\omega\pi x)\sin(\omega\pi y)\exp(-\omega\pi t) \end{pmatrix},$$
$$E_z = \sin(\omega\pi x)\sin(\omega\pi y)\exp(-\omega\pi t),$$
$$\boldsymbol{K} \equiv \begin{pmatrix} K_x \\ K_y \end{pmatrix} = \omega\pi\begin{pmatrix} \sin(\omega\pi x)\cos(\omega\pi y)\exp(-\omega\pi t) \\ -\cos(\omega\pi x)\sin(\omega\pi y)\exp(-\omega\pi t) \end{pmatrix},$$
$$J_z = \omega\pi\sin(\omega\pi x)\sin(\omega\pi y)\exp(-\omega\pi t),$$

which leads to source terms

$$f = -2\omega\pi\sin(\omega\pi x)\sin(\omega\pi y)\exp(-\omega\pi t),$$
$$g_x = K_x, \qquad g_y = K_y.$$

Table 3
Example 2. L_∞ and L_2 errors for magnetic field H_x with linear basis function and $\tau = 10^{-8}$ at 1000 time steps.

	$h = 1/5$	$h = 1/10$	Rates	$h = 1/20$	Rates	$h = 1/40$	Rates	$h = 1/80$	Rates
L_∞ errors	1.6979e–4	1.2971e–4	0.3885	7.3808e–5	0.8134	3.8803e–5	0.9276	1.9643e–5	0.9822
L_2 errors	5.3631e–5	3.6010e–5	0.5747	1.9377e–5	0.8941	9.8288e–6	0.9793	4.9160e–6	0.9995

Table 4
Example 2. L_∞ and L_2 errors for magnetic field H_x with quadratic basis function and $\tau = 10^{-8}$ at 1000 time steps.

	$h = 1/5$	$h = 1/10$	Rates	$h = 1/20$	Rates	$h = 1/40$	Rates	$h = 1/80$	Rates
L_∞ errors	1.7836e–4	5.9329e–5	1.5880	1.5958e–5	1.8945	4.1534e–6	1.9419	1.0931e–6	1.9259
L_2 errors	2.9229e–5	9.1135e–6	1.6813	2.3892e–6	1.9315	6.0817e–7	1.9740	1.5630e–7	1.9602

Table 5
Example 2. L_∞ and L_2 errors for magnetic field H_x with cubic basis function and $\tau = 10^{-12}$ at one time step.

	$h = 1/5$	$h = 1/10$	Rates	$h = 1/20$	Rates	$h = 1/40$	Rates	$h = 1/80$	Rates
L_∞ errors	9.5958e–12	1.4932e–12	2.6840	2.0184e–13	2.8871	2.5757e–14	2.9702	3.2474e–15	2.9876
L_2 errors	1.2339e–12	1.8039e–13	2.7740	2.3722e–14	2.9268	2.9871e–15	2.9894	3.7331e–16	3.0003

Table 6
Example 2. L_∞ and L_2 errors for magnetic field H_x with cubic basis function and $\tau = 10^{-12}$ at 1000 time step.

	$h = 1/5$	$h = 1/10$	Rates	$h = 1/20$	Rates	$h = 1/40$	Rates	$h = 1/80$	Rates
L_∞ errors	9.5958e–9	1.4933e–9	2.6839	2.0183e–10	2.8873	2.5762e–11	2.9698	3.2503e–12	2.9866
L_2 errors	1.2339e–9	1.8039e–10	2.7740	2.3721e–11	2.9269	2.9867e–12	2.9895	3.7260e–13	3.0029

Table 7
Example 2. L_∞ and L_2 errors for magnetic field H_x with quadratic basis function, $\tau = 0.01h$ and $nt = 10/h$ time steps.

	$h = 1/5$	$h = 1/10$	Rates	$h = 1/20$	Rates	$h = 1/40$	Rates	$h = 1/80$	Rates
L_∞ errors	0.6144	0.1807	1.7656	0.0394	2.1973	0.0112	1.8147	0.0028	2.0
L_2 errors	0.0810	0.0216	1.9069	0.0042	2.3626	9.7398e–004	2.1084	2.4353e–004	1.9998

Many numerical tests have been carried out for various h, τ and ω. Selected results are presented for $\omega = 4$ in Tables 3, 4, which again justify the theoretical convergence rate $O(\tau^2 + h^r)$ for a r-th order basis function when $r \leqslant 2$. When $r \geqslant 3$, we need smaller time steps in order to see the spatial convergence rate clearly, since the error will be saturated when the mesh is fine enough. In Tables 5, 6, we presented the results obtained with $\omega = 4$, $r = 3$, $\tau = 10^{-12}$ at 1 and 1000 time steps, respectively. Tables 5, 6 show the convergence rate $O(h^3)$ clearly.

Finally, we present a test for checking the time convergence rate $O(\tau^2)$. Since the time step depends on h, we cannot check this using the traditional way by fixing a very small h with various τ. Here we solve the problem with quadratic basis function and $\omega = 4$. We fix $\tau = 0.01h$, and the final time $T = 0.1$ (i.e., the number of time step varies as $nt = 10/h$). A representative result is listed in Table 7, which clearly shows $O(\tau^2)$ rate. This result is consistent with the theoretical analysis, since in this case $O(\tau^2 + h^2) = O(\tau^2)$ when we fix $\tau = 0.01h$.

Remark 4.1. We like to remark that it seems impossible to construct an accurate moving wave solution (i.e., $\boldsymbol{E}$ or $\boldsymbol{H}$ has time-dependence as $\sin(\omega t)$ or $\cos(\omega t)$) for the metamaterial model, since the metamaterial is a dispersive lossy medium. This fact can be seen from the system (65)–(70). Substituting solution $E_z(x, y, t) = p(x, y)\sin\omega t$ into (68), we have

$$J_z(x, y, t) = e^{-\Gamma_e t} J_z(0) - \omega_e^2 p(x, y)\left[\frac{1}{\Gamma_e^2 + \omega^2}(\Gamma_e \sin\omega t - \omega\cos\omega t) + \frac{\omega}{\Gamma_e^2 + \omega^2} e^{-\Gamma_e t}\right],$$

which cannot satisfy (67) unless choosing source term $f = J_z$. However, such a solution does not represent the feature of dispersive media, since the induced currents are decoupled from the electric and magnetic fields. Unfortunately, this is exactly what Lanteri and Scheid [13] did in their numerical example for a simple dispersive medium model. It is easy to see that the right hand side term of the third equation of (5.5) in [13] becomes zero for the exact solution given there, hence the polarization represented by the fourth equation of (5.5) does not affect the electric and magnetic fields anymore.

4.2. Example 3: Wave propagation in a rectangular metamaterial slab

Here we consider a wave propagation model originally introduced and solved by FDTD method by Ziolkowski [27]. In this example, a metamaterial slab is chosen to be $[0.024, 0.054]m \times [0.002, 0.062]m$, which is located inside a vacuum with dimension $[0, 0.07]m \times [0, 0.064]m$. The vacuum is surrounded by a PML with thickness $dd = 12h$, where h denotes the mesh size. The 2-D transverse magnetic PML model can be obtained from (51)–(54):

$$\begin{aligned}
\mu_0 \frac{\partial H_x}{\partial t} &= -\frac{\partial E_z}{\partial y} - K_x + \mu_0(\sigma_x - \sigma_y)H_x,\\
\mu_0 \frac{\partial H_y}{\partial t} &= \frac{\partial E_z}{\partial x} - K_y - \mu_0(\sigma_x - \sigma_y)H_y,\\
\epsilon_0 \frac{\partial E_z}{\partial t} &= \frac{\partial H_y}{\partial x} - \frac{\partial H_x}{\partial y} - J_z - \epsilon_0(\sigma_x + \sigma_y)E_z,\\
\frac{\partial J_z}{\partial t} &= \epsilon_0 \sigma_x \sigma_y E_z,\\
\frac{\partial K_x}{\partial t} &= -\sigma_x K_x + \mu_0(\sigma_x - \sigma_y)\sigma_x H_x,\\
\frac{\partial K_y}{\partial t} &= -\sigma_y K_y - \mu_0(\sigma_x - \sigma_y)\sigma_y H_y,
\end{aligned}$$

where the subscripts 'x, y' and 'z' denote the corresponding components in the x, y and z directions, respectively.

The incident source wave is imposed as E_z field and is excited at $x = 0.004m$ and $y \in [0.025, 0.035]m$. The source wave varies in space as $e^{-(x-0.03)^2/(50h)^2}$ and in time as [27]:

$$f(t) = \begin{cases} 0, & \text{for } t < 0,\\ g_1(t)\sin(\omega_0 t), & \text{for } 0 < t < mT_p,\\ \sin(\omega_0 t), & \text{for } mT_p < t < (m+k)T_p,\\ g_2(t)\sin(\omega_0 t), & \text{for } (m+k)T_p < t < (2m+k)T_p,\\ 0, & \text{for } t > (2m+k)T_p, \end{cases}$$

where we denote $T_p = 1/f_0$, and

$$\begin{aligned}
g_1(t) &= 10x_1^3 - 15x_1^4 + 6x_1^5, \quad x_1 = t/mT_p,\\
g_2(t) &= 1 - \left(10x_2^3 - 15x_2^4 + 6x_2^5\right), \quad x_2 = \left(t - (m+k)T_p\right)/mT_p.
\end{aligned}$$

In our simulation, we use $m = 2, k = 100$.

The damping function σ_x and σ_x are chosen as a fourth-order polynomial function, more specifically, we choose:

$$\sigma_x(x, y) = \begin{cases} \sigma_{\max}(\frac{x-0.07}{dd})^4 & \text{if } x \geqslant 0.07\\ \sigma_{\max}(\frac{|x|}{dd})^4 & \text{if } x \leqslant 0.0\\ 0 & \text{elsewhere,} \end{cases}$$

where $\sigma_{max} = -\log(err) * 5 * 0.07 * c_v/(2 * dd)$ with $err = 10^{-7}$. Function σ_y has the same form but varies with respect to the y variable.

An unstructured triangular mesh with 14586 triangles and 7422 nodes is used for our simulation. Furthermore, the quadratic basis function, mesh size $h = 2 \cdot 10^{-4}$ and time step size $\tau = 0.1$ ps are used. The mesh and the absolute value of E_z field at various times are presented in Fig. 1, which clearly shows that the wave propagates backwards in the metamaterial slab and demonstrates the re-focusing property of metamaterials. The simulation is consistent with results obtained by the FDTD method [27] and the finite element method with edge elements [12]. Moreover, the leap-frog DG method is quite efficient as evidenced by our implementation that the CPU times are 172.71 s, 342.80 s, 510.50 s, 681.63 s, and 854.14 s for 1000, 2000, 3000, 4000, and 5000 time step simulations, respectively.

4.3. Example 4: Wave propagation in a triangular metamaterial slab

The setup of this model is basically same as the last example, the only difference is that the rectangular metamaterial slab is replaced by a triangular slab with vertices $(0.024, 0.002)$, $(0.054, 0.002)$, and $(0.024, 0.062)$. A similar example was developed [12] to demonstrate Snell's Law and the negative refractive index of the metamaterial. An unstructured triangular mesh with 14600 triangles and 7429 nodes is used for this model. The mesh size $h = 2 \cdot 10^{-4}$ and the time step size $\tau = 0.1$ ps are used. The mesh and E_z fields at various times are presented in Fig. 2, which clearly shows that the wave bends toward the same side at the interface between the metamaterial and the vacuum by obeying Snell's Law. The simulation is consistent with results obtained by the lowest-order edge elements [12]. Furthermore, the leap-frog DG method seems

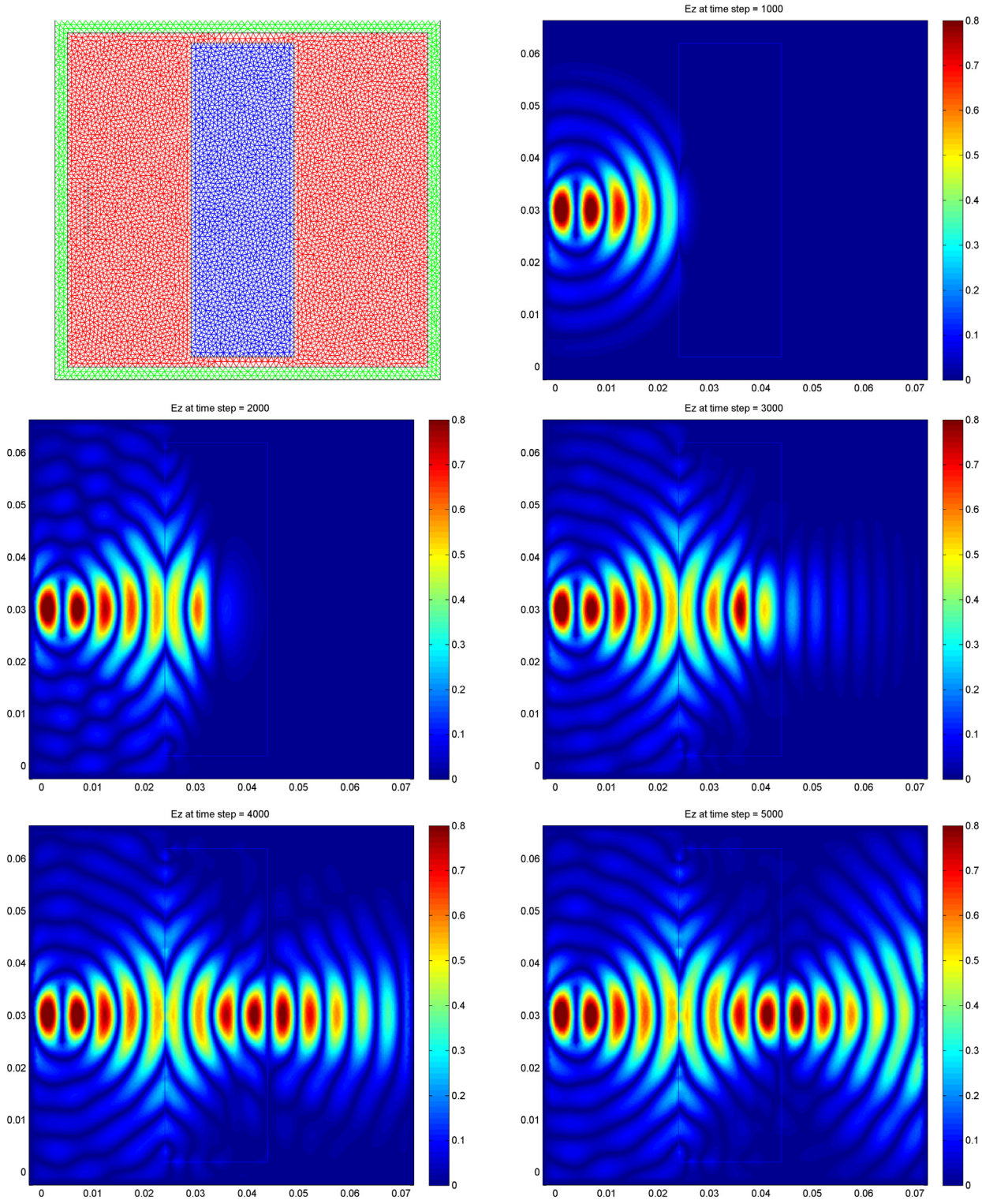

Fig. 1. Example 3. The mesh and contour plots of $|E_z|$ obtained with $h = 2 \cdot 10^{-4}$, $\tau = 0.1$ ps at 1000, 2000, 3000, 4000, and 5000 time steps.

more powerful and efficient compared to our edge element implementation with a hybrid grid of triangles and rectangles, since current implementation can use arbitrary order basis functions on unstructured triangular or tetrahedral grids. The CPU times of our DG method are 173.20 s, 347.58 s, 519.39 s, 691.69 s, and 864.14 s for 1000, 2000, 3000, 4000, and 5000 time step simulations, respectively.

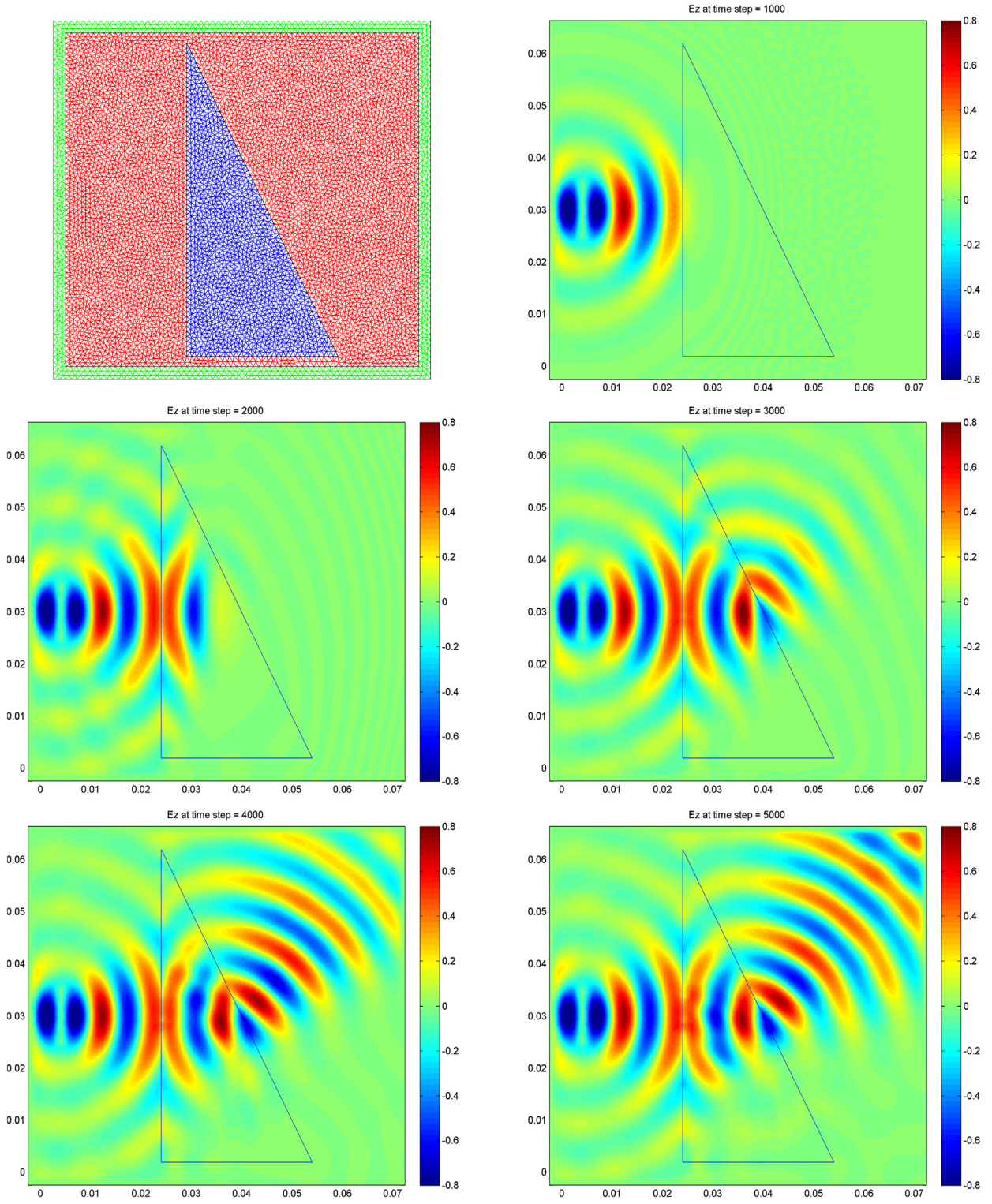

Fig. 2. Example 4. The mesh and contour plots of E_z obtained with $h = 2 \cdot 10^{-4}$, $\tau = 0.1$ ps at 1000, 2000, 3000, 4000, and 5000 time steps.

5. Conclusions

In this paper, we develop a nodal discontinuous Galerkin method for solving the time-dependent Maxwell's equations in metamaterials. We prove the numerical stability and error estimate for both semi- and fully-discrete schemes. Numerical

results with analytical solutions are first presented to support the theoretical analysis and check the correctness of our algorithmic implementation. Then two wave propagation problems are presented to illustrate the interesting backward propagation phenomenon happened when wave propagates in metamaterials.

Acknowledgements

The authors like to thank anonymous referees for their many insightful comments that improved the paper.

References

[1] D.N. Arnold, F. Brezzi, B. Cockburn, L.D. Marini, Unified analysis of discontinuous Galerkin methods for elliptic problems, SIAM J. Numer. Anal. 39 (2002) 1749–1779.
[2] B. Cockburn, G.E. Karniadakis, C.-W. Shu (Eds.), Discontinuous Galerkin Methods: Theory, Computation and Applications, Springer, Berlin, 2000.
[3] B. Cockburn, F. Li, C.-W. Shu, Locally divergence-free discontinuous Galerkin methods for the Maxwell equations, J. Comput. Phys. 194 (2004) 588–610.
[4] E.T. Chung, P. Ciarlet Jr., T.F. Yu, Convergence and superconvergence of staggered discontinuous Galerkin methods for the three-dimensional Maxwell's equations on Cartesian grids, J. Comput. Phys. 235 (2013) 14–31.
[5] V. Dolean, H. Fahs, L. Fezoui, S. Lanteri, Locally implicit discontinuous Galerkin method for time domain electromagnetics, J. Comput. Phys. 229 (2010) 512–526.
[6] L. Fezoui, S. Lanteri, S. Lohrengel, S. Piperno, Convergence and stability of a discontinuous Galerkin time-domain methods for the 3D heterogeneous Maxwell equations on unstructured meshes, Modél. Math. Anal. Numér. 39 (6) (2005) 1149–1176.
[7] F.X. Giraldo, J.S. Hesthaven, T. Warburton, Nodal high-order discontinuous Galerkin methods for the spherical shallow water equations, J. Comput. Phys. 181 (2002) 499–525.
[8] M.J. Grote, A. Schneebeli, D. Schötzau, Interior penalty discontinuous Galerkin method for Maxwell's equations: energy norm error estimates, J. Comput. Appl. Math. 204 (2007) 375–386.
[9] J.S. Hesthaven, T. Warburton, Nodal high-order methods on unstructured grids. I. Time-domain solution of Maxwell's equations, J. Comput. Phys. 181 (2002) 186–221.
[10] J.S. Hesthaven, T. Warburton, Nodal Discontinuous Galerkin Methods: Algorithms, Analysis, and Applications, Springer, New York, 2008.
[11] P. Houston, I. Perugia, A. Schneebeli, D. Schötzau, Interior penalty method for the indefinite time-harmonic Maxwell equations, Numer. Math. 100 (2005) 485–518.
[12] Y. Huang, J. Li, W. Yang, Modeling backward wave propagation in metamaterials by the finite element time domain method, SIAM J. Sci. Comput. 35 (2013) B248–B274.
[13] S. Lanteri, C. Scheid, Convergence of a discontinuous Galerkin scheme for the mixed time domain Maxwell's equations in dispersive media, IMA J. Numer. Anal. 33 (2013) 432–459.
[14] J. Li, Development of discontinuous Galerkin methods for Maxwell's equations in metamaterials and perfectly matched layers, J. Comput. Appl. Math. 236 (2011) 950–961.
[15] J. Li, Numerical convergence and physical fidelity analysis for Maxwell's equations in metamaterials, Comput. Methods Appl. Mech. Eng. 198 (2009) 3161–3172.
[16] J. Li, Y. Huang, Time-Domain Finite Element Methods for Maxwell's Equations in Metamaterials, Springer Ser. Comput. Math., vol. 43, Springer, 2013.
[17] J. Li, J.W. Waters, E.A. Machorro, An implicit leap-frog discontinuous Galerkin method for the time-domain Maxwell's equations in metamaterials, Comput. Methods Appl. Mech. Eng. 223–224 (2012) 43–54.
[18] H. Liu, J. Yan, The direct discontinuous Galerkin (DDG) methods for diffusion problems, SIAM J. Numer. Anal. 47 (2009) 675–698.
[19] T. Lu, P. Zhang, W. Cai, Discontinuous Galerkin methods for dispersive and lossy Maxwell's equations and PML boundary conditions, J. Comput. Phys. 200 (2004) 549–580.
[20] E. Montseny, S. Pernet, X. Ferriéres, G. Cohen, Dissipative terms and local time-stepping improvements in a spatial high order discontinuous Galerkin scheme for the time-domain Maxwell's equations, J. Comput. Phys. 227 (2008) 6795–6820.
[21] J. Qiu, B.C. Khoo, C.-W. Shu, A numerical study for the performance of the Runge–Kutta discontinuous Galerkin method based on different numerical fluxes, J. Comput. Phys. 212 (2006) 540–565.
[22] D.R. Smith, W.J. Padilla, D.C. Vier, S.C. Nemat-Nasser, S. Schultz, Composite medium with simultaneously negative permeability and permittivity, Phys. Rev. Lett. 84 (2000) 4184–4187.
[23] S. Sun, B. Riviére, M.F. Wheeler, A combined mixed finite element and discontinuous Galerkin method for miscible displacement problem in porous media, in: Tony F. Chan, Yunqing Huang, Tao Tang, Jinchao Xu, Lung-an Ying (Eds.), Recent Progress in Computational and Applied PDES: Conference Proceedings for the International Conference Held in Zhangjiajie in July 2001, Springer, 2003, pp. 323–352.
[24] E. Turkel, A. Yefet, Absorbing PML boundary layers for wave-like equations, Appl. Numer. Math. 27 (1998) 533–557.
[25] B. Wang, Z. Xie, Z. Zhang, Error analysis of a discontinuous Galerkin method for Maxwell equations in dispersive media, J. Comput. Phys. 229 (2010) 8552–8563.
[26] R.W. Ziolkowski, Maxwellian material based absorbing boundary conditions, Comput. Methods Appl. Mech. Eng. 169 (1999) 237–262.
[27] R.W. Ziolkowski, Pulsed and CW Gaussian beam interactions with double negative metamaterial slabs, Opt. Express 11 (2003) 662–681.